Theory of domain patterns in systems with long-range interactions of Coulomb type

C. B. Muratov*
Department of Mathematical Sciences, New Jersey Institute of Technology, Newark, New Jersey 07102
(Received 27 March 2002; published 10 December 2002)

We develop a theory of the domain patterns in systems with competing short-range attractive interactions and long-range repulsive Coulomb interactions. We take an energetic approach, in which patterns are considered as critical points of a mean-field free energy functional. Close to the microphase separation transition, this functional takes on a universal form, allowing us to treat a number of diverse physical situations within a unified framework. We use asymptotic analysis to study domain patterns with sharp interfaces. We derive an interfacial representation of the pattern's free energy which remains valid in the fluctuating system, with a suitable renormalization of the Coulomb interaction's coupling constant. We also derive integro-differential equations describing stationary domain patterns of arbitrary shapes and their thermodynamic stability, coming from the first and second variations of the interfacial free energy. We show that the length scale of a stable domain pattern must obey a certain scaling law with the strength of the Coulomb interaction. We analyzed the existence and stability of localized (spots, stripes, annuli) and periodic (lamellar, hexagonal) patterns in two dimensions. We show that these patterns are metastable in certain ranges of the parameters and that they can undergo morphological instabilities leading to the formation of more complex patterns. We discuss nucleation of the domain patterns by thermal fluctuations and pattern formation scenarios for various thermal quenches. We argue that self-induced disorder is an intrinsic property of the domain patterns in the systems under consideration.

DOI: 10.1103/PhysRevE.66.066108 PACS number(s): 05.70.Np, 64.60.My, 82.35.Jk, 47.54.+r

I. INTRODUCTION

Pattern formation is a beautiful example of cooperative behavior in complex systems. It is most pronounced in open dissipative systems maintained away from thermal equilibrium by external fluxes of energy or matter [1–6]. At the same time, there exist a great number of systems interacting with the outside world only through contact with a heat bath which are also capable of pattern formation and self-organization. Typically, these systems are characterized by the presence of coexisting phases, or a phase transition that is the driving force for the cooperative behavior. Examples of such classical systems include ferroelectric and ferromagnetic films, ferrofluids, Langmuir monolayers, various polymer systems, etc. (see, for example, [7–12]). Among such quantum systems are type-I superconductors in the intermediate state, high-temperature superconductors, degenerate ferromagnetic semiconductors, etc. (see, for example, [13–16]).

In systems not far from thermal equilibrium, patterns may form as a result of the competition of interactions operating on different length scales [7]. Typically, a short-range attractive interaction in the system would favor macroscopic phase separation. The latter, however, is counteracted by a long-range repulsive interaction. This is often accompanied by a microphase separation transition, which leads to spontaneous formation of patterns in ideally homogeneous systems upon variation of the control parameters.

An important class of systems with competing interactions are systems in which the long-range interaction is Coulombic. The fundamental nature of the Coulomb interaction makes this class of systems extremely diverse. These systems include a variety of polymer systems, such as block copolymers [10,12,17–19], weakly charged polyelectrolyte solutions [20–22], cross-linked polymer mixtures [23], amphiphile solutions [24], phase-separating ceramic compounds [25], systems undergoing reaction-controlled spinodal decomposition [26]; photostimulated phase transitions [2,14,27], etc. Some aspects of systems with competing interactions are shared by systems far from thermal equilibrium, such as heated electron-hole and gas plasmas, semiconductor devices [2,5], crystal surfaces undergoing laser-induced melting [28], autocatalytic chemical reactions, and surface catalytic reactions [4,29]. Furthermore, a number of quantum systems, such as degenerate magnetic semiconductors and high-temperature superconductors, which exhibit electronic phase separation, can be considered as systems with competing Coulomb interactions [15,30]. In addition, the general problem of Wigner crystallization [13,31], as well as the thermodynamic and glassy properties of spin systems frustrated by Coulomb interaction [30,32–36], can be considered from this point of view.

Here we develop a theory of patterns with sharp interfaces (domains) in systems with short-range attractive interactions and long-range repulsive Coulomb interactions. Our starting point is a mean-field free energy functional, which has a nonlocal term associated with the Coulomb interaction. Specifically, we are interested in the case of a weak Coulomb interaction, when domain patterns with sharp interfaces are realized. We view patterns as critical points of the free energy functional. Our main tool in the analysis is singular perturbation theory based on the strong separation of length scales in the systems under consideration. We use the results of our analysis of the domain patterns to study the nucleation and formation of complex patterns. We also discuss the effect

*Electronic address: muratov@njit.edu

of thermal fluctuations and the thermodynamic properties of these systems.

Our paper is organized as follows. In Sec. II, we introduce the general free energy functional and its reduction near a ''local'' critical point, derive the interfacial representation of the free energy, and develop a renormalization scheme to account for the effect of thermal fluctuations. In Sec. III we derive the asymptotic equations for the stationary patterns and their stability. In Sec. IV we perform a detailed analysis of localized and periodic patterns in two dimensions. In Sec. V we discuss the nucleation and growth of complex patterns as a result of instabilities of simple patterns, and in Sec. VI we draw conclusions. This paper is partially based the author's Ph.D. thesis.

II. SYSTEMS WITH COMPETING INTERACTIONS OF COULOMB TYPE

A. Free energy functional

We start by considering the following general mean-field free energy functional:

$$F=\int d^dx\left(\frac{|\nabla\phi|^2}{2}+f(\phi)+\frac{\alpha}{2}\int d^dx' g[\phi(x)] \times G(x-x')g[\phi(x')]\right). \tag{1}$$

Here $\phi(x)$ is a scalar order parameter, $f(\phi)$ is a double-well potential, $G(x-x')$ is a positive-definite long-range kernel, α is a (positive) coupling constant, $g(\phi)$ is a monotonic function that is equal to zero at some $\phi=\overline{\phi}$, and d is the dimensionality of space. Here and henceforth we use dimensionless units.

The functional in Eq. (1) may be applicable to a variety of systems. Generally, ϕ may stand for magnetization, density of the charged polymer in a polyelectrolyte solution, volume fraction of a block copolymer in a diblock copolymer melt, density of electrons or holes in a charge density wave, structural state of a catalytic surface, concentration of a chemical species, etc. [15,17,18,21,27,29,30,38]. The kernel $G(x-x')$ we are interested in is the *Coulomb* potential, i.e., it satisfies

$$-\nabla^2 G(x-x')=\delta^{(d)}(x-x'), \tag{2}$$

where $\delta^{(d)}(x)$ is the d-dimensional Dirac delta function. The physical nature of the Coulomb interaction may also significantly vary from system to system: it may arise as a result of the actual electrostatic repulsion due to charges associated with the order parameter, it may have an entropic origin, as in block copolymers, or it can come from the diffusion of chemically reacting species (see, for example, [2,17,18,21,25–30,38]). Note that in quantum systems Eq. (1) arises within the framework of density functional theory [31,39,40].

The long-ranged nature of $G(x-x')$ from Eq. (2) is expressed in the fact that its Fourier transform has a singularity at wave vector $\mathbf{k}=0$. At the same time, this Fourier transform is bounded at large k vectors. Let us emphasize that $G(x-x')$ represents a *repulsive* long-range interaction. Therefore, the Coulomb long-range interaction represented by $G(x-x')$ is *competing* with the short-range interactions represented by the first two terms in Eq. (1). It is also clear that since the Fourier transform of $G(x-x')$ is positive for all wave vectors, the functional in Eq. (1) is bounded from below on any finite domain.

If we formally put $\alpha=0$ in Eq. (1), we will recover the standard free energy functional that is used in the studies of phase separation (see, for example, [41]). On the other hand, no matter how small the value of α is, because of the singularity of the Fourier transform of $G(x-x')$ at $\mathbf{k}=0$ the effect of the long-range interaction will remain significant on sufficiently large length scales. Indeed, if the system has a finite size L, from dimensional considerations the contribution of the Coulomb interaction to the free energy will scale as αL^{d+2}. If the value of α is decreased while L remains fixed, the contribution of the Coulomb interaction goes away. This means that when $\alpha\ll 1$ the system behaves locally as if it did not have the long-range interaction. On the other hand, for an infinite system this interaction is always relevant since its contribution scales as $L^{d+2}>L^d$. Therefore, for

$$\alpha\ll 1 \tag{3}$$

the long-range interaction will be a *singular perturbation*, globally affecting the behavior of the system. It is in this case that domain patterns form in systems with a free energy of the form of Eq. (1). Since we are interested in the domain patterns here, Eq. (3) will be assumed from now on. Note that this condition is satisfied in many systems with long-range interactions of Coulomb type [15,17,18,21,23,24,30].

The singularity of $G(x-x')$ on the large length scales implies that the Fourier component of $g(\phi)$ at $\mathbf{k}=\mathbf{0}$ must vanish in order for the last integral in Eq. (1) to remain finite. This corresponds to overall electroneutrality for systems in which the order parameter is associated with the electric charge. The only possible *homogeneous* phase of the system is, therefore, $\phi=\overline{\phi}$. Thus, due to the long-range interaction global phase separation in the system becomes impossible. On the other hand, as we will see below, the system described by the free energy functional from Eq. (1) may be in a *patterned* state. By patterned states (more precisely, by stationary patterns), we mean the inhomogeneous distributions of the order parameter that are critical points of the functional F.

B. The microphase separation transition

Let us assume that in the absence of the long-range interaction the system would possess a critical point at temperature $T=T_c$. Then, in the vicinity of T_c the function $f(\phi)$ can be expanded as

$$f\simeq\frac{a\tau\phi^2}{2}+\frac{b\phi^4}{4}, \tag{4}$$

where $\tau=(T-T_c)/T_c$ is the reduced temperature, and a and b are positive constants [42]. In the following, we will talk

about T_c as the "local" critical temperature. Near T_c, the value of $|\phi| \sim \phi_0 = (a|\tau|/b)^{1/2} \ll 1$ [42]. If also $|\overline{\phi}| \ll 1$, we can expand the function $g(\phi)$ in a Taylor series and retain only the first term, so $g(\phi) \simeq \text{const} \times (\phi - \overline{\phi})$. Then, rescaling the order parameter and length with the values of ϕ_0 and the short-range correlation length $\xi = |a\tau|^{-1/2}$ [42], we can write the free energy from Eq. (1) below T_c in the following *universal* form:

$$F = \int d^d x \left(\frac{|\nabla \phi|^2}{2} - \frac{\phi^2}{2} + \frac{\phi^4}{4} + \frac{\epsilon^2}{2} \int d^d x' [\phi(x) - \overline{\phi}] \times G(x - x') [\phi(x') - \overline{\phi}] \right), \tag{5}$$

where we absorbed a constant factor into the definition of F. Here the parameter ϵ, which plays the role of the effective coupling constant of the long-range interaction, is given by

$$\epsilon = \alpha^{1/2} \left| \frac{g'(0)}{a\tau} \right| \sim \alpha^{1/2} |\tau|^{-1}. \tag{6}$$

Notice that in Eq. (5) the value of $\overline{\phi}$ has been rescaled as well, so it now depends on temperature:

$$\overline{\phi} \propto |\tau|^{-1/2}. \tag{7}$$

Also, as was discussed above, for Eq. (5) the singularity of $G(x - x')$ at small wave vectors implies that the total amount of the order parameter must be conserved (the "electroneutrality" condition):

$$\frac{1}{V} \int \phi \, d^d x = \overline{\phi}, \tag{8}$$

where V is the system's volume.

Let us consider small fluctuations of the order parameter $\delta\phi = \phi - \overline{\phi}$ away from the homogeneous phase for $T < T_c$. From the second variation of F from Eq. (5), the Fourier transform of the pair correlation function of such fluctuations is

$$\langle |\delta\phi_{\mathbf{k}}|^2 \rangle \propto \frac{V}{|\mathbf{k}|^2 + 3\overline{\phi}^2 - 1 + \epsilon^2 |\mathbf{k}|^{-2}}. \tag{9}$$

This correlation function has a maximum at nonzero k vectors with $|\mathbf{k}| = k_c$, where

$$k_c = \epsilon^{1/2}. \tag{10}$$

The fluctuations at k_c diverge when $\overline{\phi} = \pm |\overline{\phi}_c|$, where

$$|\overline{\phi}_c| = \frac{1}{\sqrt{3}} \left(1 - \frac{\epsilon}{\epsilon_c} \right)^{1/2}, \quad \epsilon_c = \frac{1}{2}. \tag{11}$$

The divergence of the fluctuations at $|\mathbf{k}| = k_c$ signifies an instability of the homogeneous phase and leads to *microphase separation* [7]. Note that the instability can only be realized if ϵ is small enough; in terms of temperature, it occurs at T slightly below T_c when Eq. (3) holds [see Eq. (6)].

As the temperature is decreased, the value of ϵ gets smaller. Note that for small α one can still be close to T_c and yet have $\epsilon \ll 1$. In this situation the long-range interaction can be a singular perturbation (in the sense discussed earlier) even in the vicinity of the transition. As was already mentioned, this is a necessary condition for the existence of the domain patterns, so below we will concentrate on the case $\epsilon \ll 1$. For $\epsilon \ll 1$ the instability of the homogeneous phase occurs close to the classical spinodal of the Ginzburg-Landau free energy: $|\overline{\phi}_c| \simeq 1/\sqrt{3}$ [see Eq. (11)]. In this case, according to Eq. (10), the instability occurs at $k_c \ll 1$.

There are two regions in the k space in which the fluctuations of the order parameter around the homogeneous phase, with $|\overline{\phi}| > |\overline{\phi}_c|$, behave differently when $\epsilon \ll 1$. According to Eq. (9), for $|\mathbf{k}| \sim 1$ one could neglect the long-range contribution, so the fluctuations $\langle |\delta\phi_{\mathbf{k}}|^2 \rangle \propto V/(|\mathbf{k}|^2 + m^2)$, where $m^2 = 3\overline{\phi}^2 - 1$, are those of the (mean-field) critical phenomena [42], with the length scale independent of ϵ:

$$l \sim 1. \tag{12}$$

On the other hand, for $|\mathbf{k}| \ll 1$ one can neglect the $|\mathbf{k}|^2$ term, so the fluctuations behave like $\langle |\delta\phi|^2_{\mathbf{k}} \rangle \propto V/(m^2 + \epsilon^2 |\mathbf{k}|^{-2}) = (V/m^2)[1 - \epsilon^2/(\epsilon^2 + m^2 |\mathbf{k}|^2)]$. The first term in this expression represents local order parameter fluctuations, while the second is the familiar Debye-Hückel correlation function [42]. The length scale associated with the latter is the *screening* length

$$L \sim \epsilon^{-1}. \tag{13}$$

For $\epsilon \ll 1$ the (generally, metastable) equilibrium state of the system should be a *domain pattern* made up of domains of large size $\sim R$ separated by narrow domain walls of width $\sim l$. Clearly, the long-range interaction cannot significantly affect the local profiles of the order parameter; however, it can affect the *locations* of the domain walls. The size of the domains will be determined by the competition between the surface energy of the domain walls $\sim R^{d-1}$ per droplet and the energy of the long-range interaction $\sim \epsilon^2 R^{d+2}$, so the characteristic size of the equilibrium domain pattern will be of order (in the context of block copolymers, see also [18])

$$R \sim \epsilon^{-2/3}. \tag{14}$$

Note that this result for the global minimizers of the sharp interface limit of Eq. (5) was recently proved by Choksi [43]. Choksi also obtained rigorous upper and lower bounds on the energy of global minimizers of Eq. (5) in the situation when the screening effects are negligible.

According to Eq. (10), the wavelength of the fluctuations with respect to which the instability of the homogeneous phase is realized is

$$\lambda = 2\pi / k_c \sim \epsilon^{-1/2}. \tag{15}$$

Comparing all these length scales, one can see that for $\epsilon \ll 1$ the following hierarchy holds:

$$l \ll \lambda \ll R \ll L. \tag{16}$$

This is a crucial property of systems with weak long-range Coulomb interaction.

C. Interfacial representation of the free energy

The solutions of the Euler-Lagrange equation obtained from Eq. (5) may be analyzed by singular perturbation theory in the asymptotic limit $\epsilon \to 0$. We perform this analysis in Sec. III A. Now, however, we use a different method which gives the free energy of the domain pattern in terms of the locations of the domain interfaces [37]. This method was used by Goldstein, Muraki, and Petrich for a reaction-diffusion system with a weak activator-inhibitor coupling [44,45]. Here we develop a procedure allowing one to calculate the free energy of a domain pattern that takes into account the screening effects.

Because of the strong separation of length scales we can introduce the following ansatz for the distribution of the order parameter:

$$\phi(x) = \phi_{\mathrm{sh}}(x) + \phi_{\mathrm{sm}}(x), \tag{17}$$

where ϕ_{sh} represents the sharp distributions, whose characteristic length of variation is of the order of the domain wall width (which in our units is of order 1), and ϕ_{sm} represents the smooth distributions, whose characteristic length of variation is comparable to the domain size R. The distribution ϕ_{sh} is chosen in such a way that it is equal to $+1$ inside the positive domains and -1 outside, whereas at the interfaces it is close to the one-dimensional domain wall of Ginzburg-Landau theory [46]:

$$\phi_{\mathrm{sh}} = \tanh\frac{\rho}{\sqrt{2}}, \tag{18}$$

where ρ is the distance from a given point to the interface, which is positive (negative) in the positive (negative) domains. Thus, the location of the interface is built into the definition of ϕ_{sh}. The contribution from ϕ_{sh} to the free energy, coming from the integration in Eq. (5) in the vicinity (of order 1) of the interfaces, gives the surface energy

$$F_{\mathrm{surf}} = \sigma_0 \oint dS, \quad \sigma_0 = 2\frac{2\sqrt{2}}{3}. \tag{19}$$

Here the surface integral gives the total surface area of the domain interfaces and σ_0 is the surface tension coefficient of the domain wall in Ginzburg-Landau theory [46].

To find the smooth distributions ϕ_{sm} away from the interfaces, we minimize the free energy in these regions. Taking into account that ϕ_{sm} varies slowly on a length scale of order 1, we can neglect the $\nabla^2\phi$ term arising in the Euler-Lagrange equation and obtain

$$\mu + \phi - \phi^3 - \epsilon^2 \int d^d x' G(x-x')[\phi(x') - \overline{\phi}] = 0, \tag{20}$$

where μ is the chemical potential (a constant) coming from the constraint given by Eq. (8). On the scale of the domains, $\phi_{\mathrm{sh}} = \pm 1$ away from the interfaces. We will assume that inside the domains $|\phi_{\mathrm{sm}}| \ll 1$, which is justified for $R \ll \epsilon^{-1}$ (see below). This allows us to linearize Eq. (20) around ϕ_{sh} away from the interfaces. Using Eq. (17) with $\phi_{\mathrm{sh}}^2 = 1$, Eq. (20) is written as

$$\phi_{\mathrm{sm}} = -\kappa^2\psi, \quad \kappa^2 = \frac{1}{2}, \tag{21}$$

where we introduced an effective field

$$\psi = -\mu + \epsilon^2 \int d^d x' G(x-x')[\phi_{\mathrm{sh}}(x') + \phi_{\mathrm{sm}}(x') - \overline{\phi}]. \tag{22}$$

Note that the constant κ^2 is basically the coefficient of linear response for the local theory.

Applying ∇^2 to Eq. (22) and using Eqs. (2) and (21), we obtain

$$-\nabla^2\psi + \epsilon^2\kappa^2\psi = \epsilon^2(\phi_{\mathrm{sh}} - \overline{\phi}). \tag{23}$$

Note that our definition of ψ, together with Eq. (21), implies that Eq. (8) is automatically satisfied to leading order in ϵ. This can be seen by integrating Eq. (23) over the volume of the system and taking into account that for no-flux or periodic boundary conditions the surface integral in the obtained expression vanishes. Also note that for the same reason μ drops out of this equation.

The solution of Eq. (23) is

$$\psi = \epsilon^2 \int d^d x' G_\epsilon(x-x')[\phi_{\mathrm{sh}}(x') - \overline{\phi}], \tag{24}$$

where G_ϵ is the screened Coulomb interaction which satisfies

$$-\nabla^2 G_\epsilon + \epsilon^2\kappa^2 G_\epsilon = \delta^{(d)}(x-x'). \tag{25}$$

It is explicitly given as

$$G_\epsilon(x-x') = \begin{cases} \dfrac{1}{2\epsilon\kappa}\exp(-\epsilon\kappa|x-x'|) & \text{in } d=1, \\ \dfrac{1}{2\pi}K_0(\epsilon\kappa|x-x'|) & \text{in } d=2, \\ \dfrac{\exp(-\epsilon\kappa|x-x'|)}{4\pi|x-x'|} & \text{in } d=3, \end{cases} \tag{26}$$

where $K_0(x)$ is the modified Bessel function. Thus, the fluctuations of the order parameter in the bulk indeed screen the interaction on the length scale $L \sim \epsilon^{-1}$. This means that the finite size effects will become unimportant if the system size is much greater than L. Notice that the value of ψ is estimated as $\psi \sim \epsilon^2 R^2 \ll 1$ for $R \ll \epsilon^{-1}$, justifying the lineariza-

tion used in the derivation. Also, according to Eqs. (21) and (17), in this situation the deviation of ϕ from ± 1 is small away from the interfaces.

Let us now calculate the contribution from the long-range interaction to the free energy. Once again, neglecting the $|\nabla\phi|^2$ term, expanding the nonlinearity in Eq. (5) around $\phi_{\rm sh}$ up to second order in $\phi_{\rm sm}$, and taking into account that $\phi_{\rm sh}^2=1$ away from the interfaces, to leading order in ϵ we can write the contribution of the long-range interaction (up to an overall constant) as follows:

$$\begin{aligned} F_{\rm long\ range} &= \int d^dx \left(\frac{1}{2\kappa^2}\phi_{\rm sm}^2 + \frac{1}{2}(\phi_{\rm sh}-\overline{\phi})(\psi+\mu) \right. \\ &\quad \left. + \frac{1}{2}\phi_{\rm sm}(\psi+\mu) \right) \\ &= \frac{\epsilon^2}{2}\int d^dx\, d^dx' [\phi_{\rm sh}(x)-\overline{\phi}] G_\epsilon(x-x') \\ &\quad \times [\phi_{\rm sh}(x')-\overline{\phi}], \end{aligned} \tag{27}$$

where we used Eqs. (8), (21), (22), and (24). One can see from this equation that the screening represented by $\phi_{\rm sm}$ enters the free energy only via $G_\epsilon(x-x')$. The integral in Eq. (27) can be transformed to an integral over the domain interfaces by using Eq. (25) and the fact that $\phi_{\rm sh}=\pm 1$ in the positive (negative) domains [45]. After calculating the respective integrals and collecting all the terms in the free energy (see Appendix A), we obtain

$$\begin{aligned} F &= \sigma_0 \oint dS - \frac{2(1+\overline{\phi})}{\kappa^2}\int_{\Omega_+} d^dx \\ &\quad + 2\epsilon^2 \int_{\Omega_+}\int_{\Omega_+} d^dx\, d^dx' G_\epsilon(x-x') \end{aligned} \tag{28}$$

$$\begin{aligned} &= \sigma_0 \oint dS - \frac{2\overline{\phi}}{\kappa^2 d}\oint dS(\vec{x}\cdot\hat{n}) \\ &\quad - \frac{2}{\kappa^2}\oint dS \oint dS'(\hat{n}\cdot\hat{n}') G_\epsilon(x-x'), \end{aligned} \tag{29}$$

where Ω_+ denotes the positive domains, $\hat{n}$ is the outward normal to the interface of Ω_+, and the surface integrals are over the interface. The first integral in Eq. (29) is the overall surface area of the interfaces, the second gives the total volume of the positive domains, and the third is the nonlocal contribution of the screened long-range interaction (note the distinction with the results of [45]). Thus, Eq. (29) gives the free energy of the domain pattern in terms of the locations of the interfaces only. Note that the unscreened version of Eq. (28) was recently derived rigorously by Ren and Wei in the context of Γ convergence [47].

D. Renormalization

The treatment above is based on the mean-field free energy functional from Eq. (5) and therefore neglects the effects of thermal fluctuations. In a fluctuating theory, this functional will become an effective Hamiltonian, in general requiring an appropriate field-theoretic treatment. Nevertheless, we propose that the effect of the critical phenomena fluctuations can be taken into account by an appropriate renormalization of the main parameters of the free energy in the interfacial regime [48].

Indeed, if one looks at the singularly perturbed [Eq. (3)] fluctuating system near T_c, on small length scales one will see critical phenomena fluctuations of a second-order phase transition *without* the long-range interaction. This will happen as long as the characteristic screening length L of the long-range interaction is much greater than the correlation length ξ of the critical phenomena fluctuations. The critical exponents associated with the local critical phenomena fluctuations must be those of the d-dimensional Ising model [42]. So the local average of the order parameter will be close to a constant, $\phi=\pm\phi_0|\tau|^\beta$, where $\tau=(T-T_c)/T_c$ is the reduced temperature and β is the corresponding critical exponent. Also, the surface tension coefficient of an interface in which the order parameter changes sign is $\sigma=\sigma_0|\tau|^{\nu(d-1)}$, where ν is another critical exponent, and its width is roughly the correlation length $\xi=\xi_0|\tau|^{-\nu}$ [42].

Observe that the long-range coupling involves integration over regions of size $\sim R$ which for the domain patterns must be much greater than the correlation length. Therefore, it is the *average* value of the order parameter that gives the main contribution to the long-range interaction energy for $R\gg\xi$. This energy has to be compared with the surface energy, so in equilibrium we obtain

$$\sigma_0|\tau|^{\nu(d-1)}R^{d-1} \sim \alpha\phi_0^2|\tau|^{2\beta}R^{d+2}. \tag{30}$$

Rescaling the order parameter and length appropriately and introducing the *renormalized* coupling constant

$$\epsilon^2 = \alpha\phi_0^2\xi_0^3|\tau|^{2\beta-\nu(d+2)}, \tag{31}$$

we can still write down the interfacial free energy of the system in the form of Eq. (29), where, as usual, we dropped the primes and neglected an overall constant factor. Caution, however, is necessary here in considering the screening effects. As was noted earlier, the constant κ appearing in the mean-field definition of the screened long-range interaction $G_\epsilon(x-x')$ is related to the coefficient of linear response for the local theory. When the critical phenomena fluctuations are taken into account, the value of κ can be calculated via the linear response function $\chi=\chi_0|\tau|^{-\gamma}$ that relates the unscaled values of $\phi_{\rm sm}$ and ψ (below T_c) [see Eqs. (21) and (22)]. After an appropriate rescaling and using the definition of ϵ from Eq. (31), we obtain that

$$\kappa^2 = \frac{\chi_0}{\phi_0^2\xi_0}, \tag{32}$$

which is a constant of order 1, independent of temperature. In writing Eq. (32) we used the scaling relation $2\beta+\gamma-d\nu=0$ between the critical exponents [42].

Thus, we can renormalize the parameter ϵ and redefine the parameter κ to obtain once again the free energy of a domain pattern in the form of Eq. (29) even in the case of a system locally experiencing critical phenomena fluctuations. Let us point out that the free energy of a domain pattern of size of order $R \gg \xi$ will be much greater than $k_B T_c$ (in the unscaled units) [see Eq. (29)], since $\sigma \xi^{d-1}/k_B T_c \sim 1$ [42]. This leads us to the conclusion that in a strongly fluctuating system the domain patterns should be essentially described by the interfacial mean-field theory, and all the properties of the domains in the fluctuating system will be equivalent to those of the domains in the mean-field systems described by Eq. (5), provided that one uses the renormalization given by Eqs. (31) and (32). Thus, the universality discussed earlier for the mean-field model should in fact extend to all systems near the local critical temperature as long as the coupling constant α of the long-range interaction is small enough. Note that in this situation Eq. (5) may be used as a phase-field model representation for the free energy of the domain patterns [48].

In the renormalization of the main parameters of the system we made the assumption that the size of the domains must be much greater than the correlation length ξ. According to Eq. (14), this condition is satisfied as long as $\epsilon \ll 1$. In view of Eq. (31), this is the case when the reduced temperature τ is much lower than $\tau = -\tau_c$, where

$$\tau_c \sim \alpha^{1/[\nu(d+2)-2\beta]}, \tag{33}$$

at which $\epsilon \sim 1$. When the temperature is decreased below $-\tau_c$, the long-range interaction becomes progressively more and more relevant at long distances, until for $\tau \ll -\tau_c$ (what means $\epsilon \ll 1$) long-lived domain structures with the free energy cost of each domain $\Delta F/k_B T_c \gg 1$ will start to form. On the other hand, for $\tau \gg +\tau_c$ the long-range coupling, which scales as $\alpha\xi^2$, will be much smaller than the effective local coupling, which is of order $\chi^{-1} \sim |\tau|^{\gamma}$, so one will observe only the critical phenomena fluctuations above τ_c. It is a question whether there is a microphase separation transition from the homogeneous to the patterned phase (which is analogous to the freezing transition in liquids) or a smooth crossover from one to another in a strongly fluctuating system. It is clear, however, that the uniform phase must be thermodynamically unstable when $\tau \lesssim -\tau_c$. At the same time, at $\tau \sim -\tau_c$ the fluctuations are strong, so one can envisage the system as a collection of domains that randomly appear and disappear in different locations and move about like particles in a dense liquid. In any case, there must exist a narrow transition region $-\tau_c \lesssim \tau \lesssim \tau_c$, upon going through which the phase should change from uniform to patterned.

III. PROPERTIES OF THE DOMAIN PATTERNS

A. Equations for stationary patterns

The stationary patterns in the mean-field model introduced in Sec. II B must satisfy the Euler-Lagrange equation obtained from Eq. (5):

$$\nabla^2\phi + \phi - \phi^3 + \mu - \epsilon^2 \int d^d x' G(x-x')[\phi(x') - \overline{\phi}] = 0, \tag{34}$$

where μ is the chemical potential. Formally, this integro-differential equation can be rewritten as a pair of stationary reaction-diffusion equations of activator-inhibitor type [44,45,48,49]. Indeed, if the last term in Eq. (34) is denoted by ψ, this equation can be rewritten as

$$\nabla^2\phi + \phi - \phi^3 - \psi = 0, \tag{35}$$

$$\nabla^2\psi + \epsilon^2(\phi - \overline{\phi}) = 0, \qquad \langle\psi\rangle = -\mu, \tag{36}$$

where $\langle\cdot\rangle$ denotes averaging over the system's volume.

Reaction-diffusion equations of the type of Eqs. (35) and (36) have been studied by many authors (see, for example, [2,45,50–53]). In the limit $\epsilon \to 0$ their solutions can be treated by the methods of singular perturbation theory (matched asymptotics) [2,50,54,55]. According to singular perturbation theory, the solution ϕ of Eq. (35) can be broken up into inner and outer solutions. The inner solution varies on a length scale of order 1 and describes the variation of the order parameter in the vicinity of the domain interfaces, while the outer solution varies on a length scale R of the order of the characteristic size of the domains and describes the variation of the order parameter away from the interfaces. Similarly, the solution ψ of Eq. (36) will vary on the length scale R.

Since the variable ψ varies slowly on the inner scale, it can be considered as constant in the interface. Since the curvature of the domain wall is also much smaller than the domain wall width, to the leading order we can write Eq. (35) in the vicinity of the interface as

$$\frac{\partial^2\phi}{\partial\rho^2} - 2H\frac{\partial\phi}{\partial\rho} + \phi - \phi^3 - \psi_i = 0, \tag{37}$$

where ρ is the distance from a given point to the interface, which is positive if the point is inside the positive domain and negative otherwise, $H = \frac{1}{2}(k_1 + k_2)$ is the mean curvature of the interface (positive if the positive domain is convex; k_1 and k_2 are the principal curvatures), and ψ_i is the value of ψ on the interface. In the following, we will write all the formulas in the three-dimensional case; in two or one dimensions one has to set one or two principal curvatures of the interface, respectively, to zero.

Equation (37) can be solved exactly; its solution has the form $\phi(\rho) = a\tanh(b\rho + c)$, where a, b, and c are certain constants. This solution exists only when $2H - \frac{16}{9}H^3 = -3\psi_i/\sqrt{2}$. Since in the domain pattern $H \ll 1$, it is sufficient to linearize this equation with respect to H, so we obtain (see also [56])

$$\sigma_0 H = -\psi_i, \tag{38}$$

where σ_0 is given by Eq. (19). This, in turn, implies that $\psi \ll 1$ in order for a pattern to be stationary. Note that to leading order $\phi(\rho)$ in the interface is given by Eq. (18).

Away from the interfaces (on the outer scale) ϕ varies slowly, so one can neglect the gradient square term in Eq. (35). Then, according to Eq. (35), we have $\phi-\phi^3=\psi$. Since we must have $\psi \ll 1$, this equation can be linearized with respect to ϕ around $\phi=\pm 1$ in the positive and negative domains, respectively. So, one obtains that to leading order $\phi=\pm 1-\kappa^2\psi$ in the outer regions. Here, as in Sec. II C, we have $\kappa^2=\frac{1}{2}$. If we substitute this expression into Eq. (36), we will obtain precisely the same equation for ψ as Eq. (23), with $\phi_{\rm sh}=\pm 1$.

The solution of Eq. (23) can be written as an integral over the domain interfaces (Appendix A; see also [45,56]):

$$\psi=-\frac{1+\overline{\phi}}{\kappa^2}+\frac{2}{\kappa^2}\oint dS'\{\hat{n}'\cdot\vec{\nabla}'(G_\epsilon-G)\}, \qquad (39)$$

where $\vec{\nabla}'$ is the gradient with respect to x'. Combining this equation with Eq. (38), we obtain the following equation for the locations of the interfaces:

$$\sigma_0 H=\frac{1+\overline{\phi}}{\kappa^2}-\frac{2}{\kappa^2}\oint dS'\{\hat{n}'\cdot\vec{\nabla}'(G_\epsilon-G)\}. \qquad (40)$$

This equation can be further simplified if the distance between the points on the interface is much smaller than ϵ^{-1}. In this case one can expand G_ϵ in Eq. (40) in $\epsilon\kappa|x-x'|$ and retain the terms up to second order. It is easy to see that only the terms of second and higher orders of the expansion of G_ϵ in ϵ will give nontrivial contributions to the right-hand side of Eq. (40). Also, in view of the approximations used to derive Eq. (40), this equation is valid when the characteristic size R of the domains satisfies $1\ll R\ll\epsilon^{-1}$.

Equation (40) describes the pressure balance across the interface. Indeed, the term in the left-hand side of this equation is the Laplace law, the first term in the right-hand side gives the bulk pressure, and the second one gives the nonlocal contribution to pressure due to the interaction of the domain walls with each other.

Let us emphasize that Eq. (40) can also be straightforwardly obtained by computing the first variation of the interfacial free energy given by Eq. (29) (see Appendix A). Therefore, this equation also remains valid in the fluctuating system considered in Sec. II D. Also, note that since the solutions of Eq. (34) in the form of stationary domain patterns can be written in the form of Eq. (17) for $\epsilon\ll 1$, Eq. (29) gives the asymptotic expression for the free energy of these patterns.

B. Deformations of the domain interfaces

The solutions of the Euler-Lagrange equation given by Eq. (34) are critical points of the free energy functional from Eq. (5). Similarly, the solutions of Eq. (40) are critical points of the interfacial free energy from Eq. (29) and correspond to solutions of Eq. (34) in the limit $\epsilon\to 0$. Both these solutions define (generally metastable) stationary patterns. The question, however, arises as to when these patterns are thermodynamically *stable*. Since, apart from the nucleation phenomena discussed in Sec. V A, the effect of thermal fluctuations is small in both cases, the thermodynamic stability of the patterns is determined by the second variation of the free energy functional. Thus, the thermodynamically stable stationary patterns will be local minimizers of the free energy.

The problem of finding the second variation of the functional in Eq. (5) reduces to the calculation of the spectrum of linearization of Eq. (34). It is not difficult to see that it is equivalent to the problem of linear stability of stationary patterns in systems obeying gradient descent dynamics. Such a stability analysis in the context of general reaction-diffusion systems of activator-inhibitor type was performed in [50]. Here, instead of analyzing the second variation of F from Eq. (5), we will use the interfacial free energy from Eq. (29) for finding the spectrum of the fluctuations of the pattern's interfaces. These are, in turn, the lowest-lying modes of the spectrum and, therefore, cost the least free energy in Eq. (5). Both these approaches give the same results in the limit of small ϵ.

Let us now proceed with the calculation of the second variation of the interfacial free energy from Eq. (29). A small perturbation of the domain shape means a slight shift of the interface in the normal direction by $\rho(x)$, where x denotes a point on the interface. In terms of $\rho(x)$, the second variation of the free energy from Eq. (29) is (see Appendix A)

$$\begin{aligned}\delta^2 F=\sigma_0\oint dS\{|\nabla_\perp\rho|^2+2K\rho^2-4H^2\rho^2\}\\ +\frac{4}{\kappa^2}\oint dS\rho^2(\hat{n}\cdot\vec{\nabla})\oint dS'\{\hat{n}'\cdot\vec{\nabla}'(G_\epsilon-G)\}\\ +4\epsilon^2\oint dS\oint dS' G_\epsilon(x-x')\rho(x)\rho(x'),\end{aligned} \qquad (41)$$

where ∇' is the gradient in x', $K=k_1k_2$ is the Gaussian curvature at a given point on the unperturbed interface, $\nabla_\perp$ is the gradient along the interface, and the integration is over the unperturbed interfaces.

Different terms in the integrand of Eq. (41) represent competing tendencies that stabilize or destabilize the patterns. The $\sigma_0|\nabla_\perp\rho|^2$ term coming from the surface tension penalizes distortions of the interfaces; the term involving the curvatures $2\sigma_0(K-2H^2)\rho^2=-\sigma_0(k_1^2+k_2^2)\rho^2\leqslant 0$ is a destabilizing term coming from the curvature of the interface; the term from the second line in Eq. (41) can be rewritten as $2(\hat{n}\cdot\vec{\nabla}\psi)\rho^2$, where ψ is given by Eq. (39) (see Appendix A), and represents the change in the free energy due to the motion of the interface in the fixed effective field ψ (this term should be destabilizing also since we would generally expect the gradient of ψ to be directed inward at the interface); and the last term is the stabilizing action of the long-range interaction.

To gauge the relative strengths of these terms and determine whether a pattern is stable, we need to solve the following eigenvalue problem obtained from Eq. (41):

$L\rho=\lambda\rho$, where

$$L\rho=-\sigma_0\nabla_\perp^2\rho+2\sigma_0 K\rho-4\sigma_0 H^2\rho+2(\hat{n}\cdot\vec{\nabla}\psi)\rho$$
$$+4\epsilon^2\oint dS' G_\epsilon(x-x')\rho(x'). \quad (42)$$

The spectrum of the operator L for a stable pattern should not contain any negative eigenvalues. We will analyze the spectrum of L for simple geometries below (see also [28,45,48,50,51,57]). Now, however, let us discuss some general properties of $\delta^2 F$ in Eq. (41). It is easy to see from Eq. (41) that a typical size R in a *stable* stationary pattern must have the same scaling as that in Eq. (14) (this point was first argued in [48,50,57] based on a stability analysis of the localized and periodic patterns). Indeed, suppose a pattern is made of a collection of droplets of size and distance between each other of order R (here for definiteness we will consider three-dimensional patterns). Let us first assume that the droplets are too small, so $R\ll\epsilon^{-2/3}$. Consider a fluctuation that uniformly increases the volume of one droplet while decreasing the volume of another next to it, so that the net volume change is zero (repumping, see [2,48]). Then, if $R\ll\epsilon^{-2/3}$, the stabilizing contribution $\sim\epsilon^2 R^3$ from the last term in Eq. (41) is negligible compared to the destabilizing contribution from the curvature terms ~ 1, while the $|\nabla_\perp\rho|^2$ term is identically zero. Therefore, such a fluctuation will lead to a free energy decrease.

Now, suppose that the droplets are too big, so $R\gg\epsilon^{-2/3}$. Let us now perturb the interface of one droplet in a localized fashion in a region of size $\ell\ll R$, once again maintaining the overall volume the same (distortion [2,48,50]). Then the last term in Eq. (41), which is $\sim\epsilon^2\ell^3$, will once again be negligibly small compared to the term from the second line of Eq. (41), which is $\sim\epsilon^2\ell^2 R$. On the other hand, the gradient square term in Eq. (41), which is of order ~ 1, will not be able to compensate that contribution, if $\epsilon^{-1}R^{-1/2}\ll\ell\ll R$. Such ℓ can always be found when $R\gg\epsilon^{-2/3}$, so this kind of a fluctuation will lower the free energy, too. Note that for $R\sim\epsilon^{-1}$ this instability result was also obtained by Nishiura and Suzuki [52].

The arguments above lead to the important conclusion that (perhaps apart from some logarithmic factors; see below) the stable stationary patterns must obey the equilibrium scaling from Eq. (14), which was obtained on global energetic grounds. In other words, not only the global minimizers of the free energy [43] but all *local* minimizers must generally obey this scaling. Note, however, that these arguments do not apply in one dimension (see also [2,50,51,58]). Similarly, the equilibrium scaling from Eq. (14) is not necessarily obeyed by all stationary patterns (see for example, Secs. IV A and IV B), contrary to the statement of [59].

IV. EQUILIBRIUM PATTERNS AND MORPHOLOGICAL INSTABILITIES

Let us now use the tools developed in the preceding sections to analyze stationary domain patterns with simple geometries, such as localized and periodic patterns. In this paper, we will limit ourselves to studying two-dimensional patterns. Qualitatively the same results are expected for the more experimentally relevant three-dimensional patterns. Note, however, that the one-dimensional case is qualitatively different from those of two and three dimensions (see [2,50,58,60]).

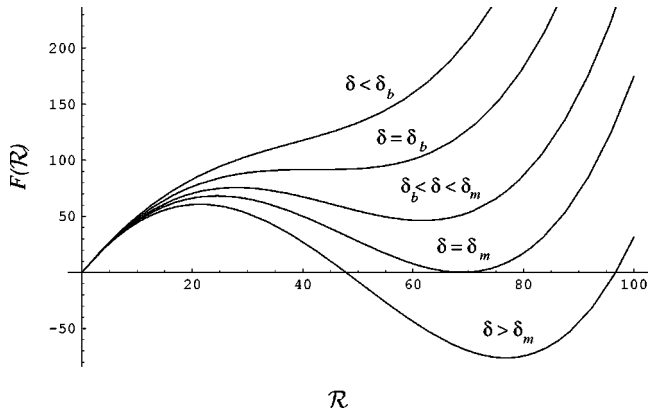

FIG. 1. The free energy of a spot for different values of $\bar{\phi}$. A plot of $F(\mathcal{R})$ from Eq. (43) with $\epsilon=0.001$, $\sigma_0=2\sqrt{2}/3$, and $\kappa=1/\sqrt{2}$. For these values of the parameters $\delta_b=0.0088$ and $\delta_m=0.0186$.

Since our system possesses a symmetry $\phi\to-\phi$, we can only consider the properties of positive domains immersed in a negative background. This means that we only need to study the region of the system's parameters in which $\bar{\phi}<0$.

A. Solitary patterns

We begin with the study of the simplest possible domain patterns: solitary patterns. In two dimensions we will consider spots, stripes, and annuli.

1. Spot

Let us first look at spots: small positive circular domains in a negative background. If the radius of the spot is much smaller than the screening length ϵ^{-1}, the interaction potential $G_\epsilon(x-x')$ in Eq. (29) can be expanded in ϵ. Retaining the terms up to ϵ^2, after a straightforward calculation we obtain that the free energy of a spot of radius $\mathcal{R}$ is asymptotically

$$F(\mathcal{R})=2\pi\sigma_0\mathcal{R}-\frac{2\pi\mathcal{R}^2\delta}{\kappa^2}-\pi\epsilon^2\mathcal{R}^4\left[\ln\left(\frac{1}{2}\epsilon\kappa\mathcal{R}\right)+\gamma-\frac{1}{4}\right], \quad (43)$$

where $\gamma\simeq 0.5772$ is the Euler constant and

$$\delta=1+\bar{\phi} \quad (44)$$

measures the degree of metastability of the homogeneous phase. The free energy of the spot given by Eq. (43) for a particular set of parameters is shown in Fig. 1.

Let us now analyze Eq. (43). First of all, when $\delta<0$, the free energy is a monotonically increasing function of $\mathcal{R}$.

When the value of δ is increased, at $\delta=\delta_b \ll 1$ a minimum and a maximum of the free energy appear (see Fig. 1). These correspond to radially stable and unstable spot solutions, with radii $\mathcal{R}=\mathcal{R}_s$ and $\mathcal{R}=\mathcal{R}_n$, respectively. At $\delta=\delta_b$ we have $\mathcal{R}_s=\mathcal{R}_n=\mathcal{R}_{\min}$. Asymptotically

$$\delta_b=\left(\frac{3}{4}\epsilon\kappa^3\sigma_0\ln^{1/2}\epsilon^{-1}\right)^{2/3}\sim\epsilon^{2/3}\ln^{1/3}\epsilon^{-1}, \tag{45}$$

$$\mathcal{R}_{\min}=\left(\frac{3\sigma_0}{4\epsilon^2\ln\epsilon^{-1}}\right)^{1/3}\sim\epsilon^{-2/3}\ln^{-1/3}\epsilon^{-1}. \tag{46}$$

This formula agrees up to the logarithmic factor with Eq. (14). These logarithmic factors are a specific feature of the two-dimensional patterns; they are absent in three dimensions [50].

When the value of δ is increased beyond δ_b, the radius $\mathcal{R}_s$ grows, while the radius $\mathcal{R}_n$ shrinks. At some value of $\delta=\delta_m\ll 1$ at which $\mathcal{R}_s=\mathcal{R}_m$, the free energy of the spot becomes negative, making the spot thermodynamically more favorable than the homogeneous phase. Once again, asymptotically,

$$\delta_m=\frac{1}{2}(3\epsilon\kappa^3\sigma_0\ln^{1/2}\epsilon^{-1})^{2/3}\sim\epsilon^{2/3}\ln^{1/3}\epsilon^{-1}, \tag{47}$$

$$\mathcal{R}_m=\left(\frac{3\sigma_0}{\epsilon^2\ln\epsilon^{-1}}\right)^{1/3}\sim\epsilon^{-2/3}\ln^{-1/3}\epsilon^{-1}. \tag{48}$$

Comparing Eqs. (45)–(48), we see that $\delta_m=2^{1/3}\delta_b$ and $\mathcal{R}_m=2^{2/3}\mathcal{R}_{\min}$.

For $\delta\gg\delta_b$ the radii $\mathcal{R}_s$ and $\mathcal{R}_n$ become asymptotically

$$\mathcal{R}_s=\left(\frac{3\delta}{\epsilon^2\kappa^2\ln\epsilon^{-1}}\right)^{1/2},\quad \mathcal{R}_n=\frac{\sigma\kappa^2}{2\delta}. \tag{49}$$

This means that, for $\delta\gg\epsilon^{2/3}\ln\epsilon^{-1}$, the radius $\mathcal{R}_s$ goes beyond the equilibrium scaling of Eq. (14). This is an indication of the morphological instability studied in Sec. IV C.

2. Annulus

Let us now analyze a pattern in the form of a thin annulus, which has radius $\mathcal{R}$ and thickness $\mathcal{L}\ll\mathcal{R}$. Calculating the free energy of such a pattern from Eq. (28), we obtain

$$F(\mathcal{R},\mathcal{L})=4\pi\sigma_0\mathcal{R}-\frac{4\pi\delta}{\kappa^2}\mathcal{R}\mathcal{L} +4\pi\epsilon^2\mathcal{R}^2\mathcal{L}^2 I_0(\epsilon\kappa\mathcal{R})K_0(\epsilon\kappa\mathcal{R}), \tag{50}$$

where $I_0(x)$ is the modified Bessel function. Minimizing this expression with respect to $\mathcal{L}$, we obtain that the value of $\mathcal{L}=\mathcal{L}_a$ in equilibrium is related to $\mathcal{R}$ as follows:

$$\mathcal{L}_a=\frac{\delta}{2\epsilon^2\kappa^2\mathcal{R}I_0(\epsilon\kappa\mathcal{R})K_0(\epsilon\kappa\mathcal{R})}. \tag{51}$$

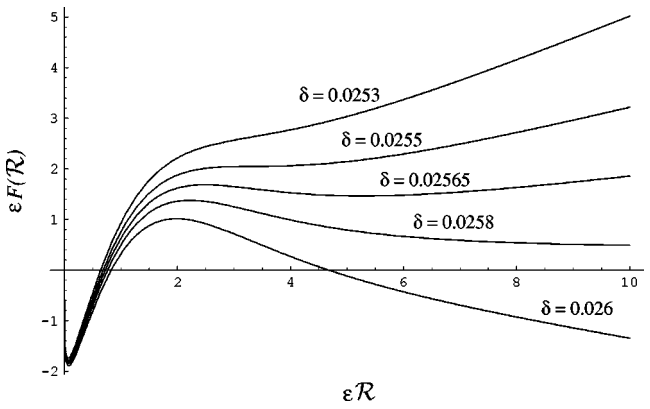

FIG. 2. The free energy of an annulus as a function of $\mathcal{R}$ for $\mathcal{L}=\mathcal{L}_a$ given by Eq. (51), obtained from Eq. (50) with $\epsilon=0.001$, $\sigma_0=2\sqrt{2}/3$, and $\kappa=1/\sqrt{2}$.

Substituting this expression into Eq. (50), we then study the critical points of F with respect to $\mathcal{R}$.

The analysis of Eqs. (50) and (51) shows that for $\delta\ll\epsilon^{1/2}$ there exists a single minimum of the free energy, corresponding to an annulus solution, whose radius and width are asymptotically

$$\mathcal{R}_a=\frac{\delta^2}{4\sigma_0\epsilon^2\kappa^4\ln^2(\epsilon\delta^{-2})},\quad \mathcal{L}_a=\frac{2\sigma_0\kappa^2}{\delta}\ln(\epsilon\delta^{-2}). \tag{52}$$

One can see that the condition $\mathcal{L}_a\ll\mathcal{R}_a$ used in the derivation of Eq. (52) is satisfied as long as $\delta\gg\epsilon^{2/3}\ln\epsilon^{-1}$.

According to Eq. (52), when $\delta\sim\epsilon^{1/2}$, we have $\mathcal{R}_a\sim\epsilon^{-1}$, so screening effects become important. The analysis of Eq. (50) shows that at some critical value of $\delta\sim\epsilon^{1/2}$ a new minimum and maximum of $F(\mathcal{R})$ appear ($\delta=0.0255$ in Fig. 2). At a slightly higher value of $\delta\sim\epsilon^{1/2}$, the second minimum of the free energy disappears ($\delta=0.0258$ in Fig. 2). The value of $\delta=\delta_\perp$ at which this happens can be easily calculated; see Eq. (54).

3. Stripe

Let us now determine the equilibrium parameters of a quasi-one-dimensional domain pattern—a stripe. A stripe of width $\mathcal{L}_s$ can be considered as the limit of an annulus as $\mathcal{R}_a\to\infty$. Using Eq. (50), we obtain that the free energy of a stripe of length $\mathcal{L}$ is

$$F=\left(2\sigma_0-\frac{\delta^2}{\epsilon\kappa^3}\right)\mathcal{L}. \tag{53}$$

The term in the parentheses characterizes the rigidity of the stripe. As can be seen from Eq. (53), this rigidity becomes negative at a critical value of $\delta=\delta_\perp$, where

$$\delta_\perp=(2\sigma_0\kappa^3\epsilon)^{1/2}. \tag{54}$$

At $\delta>\delta_\perp$ the stripe becomes unstable with respect to wriggling (see Sec. IV C).

Taking the limit $\mathcal{R}_a\to\infty$ in Eq. (51), we obtain

$$\mathcal{L}_s = \frac{\delta}{\epsilon\kappa}. \tag{55}$$

Note that the stripe solutions of Eq. (34) exist only when $\mathcal{L}_s \gtrsim \ln \epsilon^{-1}$, so to have a solution we must have $\delta \gtrsim \epsilon \ln \epsilon^{-1}$ [2,50]. Also, the width of a stripe is limited by $\mathcal{L}_s \sim \epsilon^{-1}$, in which case our linearization approximation to Eq. (20) breaks down (see also [2]). According to Eq. (55), the region of existence of stripes is wider than that of spots. Also, note that for $\delta \sim \delta_b$ (when the spot is stable), the width of the stationary stripe $\mathcal{L}_s \sim \epsilon^{-1/3} \ll \mathcal{R}_s$. This deviation from the equilibrium length scale given by Eq. (14) is essentially related to the one-dimensional nature of the stripe, for which curvature effects are absent.

B. Hexagonal and lamellar patterns

When spots or stripes are introduced into the system, the basic interaction between them is repulsion [see Eq. (28)]. In an equilibrium configuration, the domains will therefore go as far apart from each other as possible. If in the end the distance between them is greater than the screening length ϵ^{-1}, essentially they will not interact, so their behavior will be that of the solitary patterns discussed in Sec. IV A. The situation changes, however, when there are so many domains in the system that even in the close-packed arrangement the distance between them becomes less than the screening length. This is in fact a generic situation that is realized whenever the value of $\overline{\phi}$ is not close to -1 (or $\delta \sim 1$). In this case the domains will strongly interact with each other, arranging themselves into a *multidomain* pattern, so in order to decrease the energy of the long-range repulsion, the domains not only adjust their positions, but also their geometric characteristics.

Let us consider the simplest of the multidomain patterns in two dimensions, namely, periodic hexagonal and lamellar patterns. The equilibrium characteristics for several major types of periodic pattern described by Eq. (5) in the limit $\epsilon \to 0$ were found by Ohta and Kawasaki [18]. They carried out a rather involved calculation of the free energy using the Ewald summation method. Their results can be obtained by the simpler, although approximate, Wigner-Seitz method [61]. Consider a hexagonal pattern made up of circular domains, for example. In such a pattern ψ will satisfy Eq. (23) with no-flux boundary conditions on the boundaries of the hexagonal Wigner-Seitz cell. Instead of solving this problem, let us consider a single domain inside a circular cell whose area is equal to the area of the Wigner-Seitz cell (a similar approach was used in [60]). Then Eq. (23) with no-flux boundary conditions can be easily solved. Furthermore, to leading order in ϵ the screening term $\epsilon^2\kappa^2\psi$ in Eq. (23) can be neglected, if the period of the pattern $\mathcal{L}_p \ll \epsilon^{-1}$. This solution can be used to calculate the contribution from the long-range interaction to the free energy by substituting it in Eq. (27). Note that the one-dimensional analog of this method is exact, so it can also be used to calculate the free energy of the lamellar pattern.

Let the positive domains in a hexagonal pattern have radius $\mathcal{R}_s$ and period $\mathcal{L}_p \ll \epsilon^{-1}$. It is convenient to introduce the fraction f of the total area of the system occupied by positive domains. The condition of Eq. (8) implies that this fraction is related to $\overline{\phi}$ as

$$f = \frac{1+\overline{\phi}}{2}, \tag{56}$$

since inside the domains (away from the interfaces) $\phi \simeq \pm 1$ [see the discussion after Eq. (25)]. In the hexagonal pattern $\mathcal{R}_s$ and $\mathcal{L}_p$ are related via

$$\mathcal{R}_s = 3^{1/4}\mathcal{L}_p\left(\frac{1+\overline{\phi}}{4\pi}\right)^{1/2}. \tag{57}$$

From this equation one can see that, when $\overline{\phi}$ is not close to -1, the values of $\mathcal{R}_s$ and $\mathcal{L}_p$ are comparable. Note that in reality Eq. (57) is approximate, since generally the domains forming a hexagonal pattern are not ideally round. However, according to the numerical simulations, the deviations from the circular shape are very small when $\overline{\phi} < 0$, so one can safely assume the domains to be ideally circular all the way up to $\overline{\phi} = 0$.

In Eq. (57) the period of the pattern has not been specified. In fact, an infinite set of solutions in the form of hexagonal patterns with different periods exists for $-1 < \overline{\phi} < 0$ (asymptotically). All these solutions locally minimize the free energy of the system. However, among all the hexagonal patterns there is a pattern with a particular period $\mathcal{L}_p^*$ for which the value of the free energy is lowest. It is clear that, if the asymmetry between the positive and negative domains is strong, the domains will tend to form a close-packed structure, so for $\delta \ll 1$ in $d=2$ this pattern is expected to be the global minimizer of the free energy.

Using the Wigner-Seitz method, we find that the period $\mathcal{L}_p^*$ of the hexagonal pattern with the lowest free energy is (Appendix B)

$$\mathcal{L}_p^* = \epsilon^{-2/3}\left(\frac{2\pi}{f\sqrt{3}}\right)^{1/2}\left(\frac{2\sigma_0}{f-1-\ln f}\right)^{1/3}. \tag{58}$$

As ought to be expected, $\mathcal{R}_s \sim \mathcal{L}_p^* \sim \epsilon^{-2/3}$. It is interesting to note that this result agrees with the exact calculation of Ohta and Kawasaki in [18] to within 0.1% for all $f < 0.5$.

Similarly, in the case of a lamellar pattern the period $\mathcal{L}_p$ and width $\mathcal{L}_s$ of the stripe are related as

$$\mathcal{L}_s = \frac{1+\overline{\phi}}{2}\mathcal{L}_p. \tag{59}$$

A calculation analogous to the case of the hexagonal pattern shows that the period of the lamellar pattern that has the lowest free energy is given by (Appendix B)

$$\mathcal{L}_p^* = \epsilon^{-2/3}\left(\frac{6\sigma_0}{f^2(1-f)^2}\right)^{1/3}. \tag{60}$$

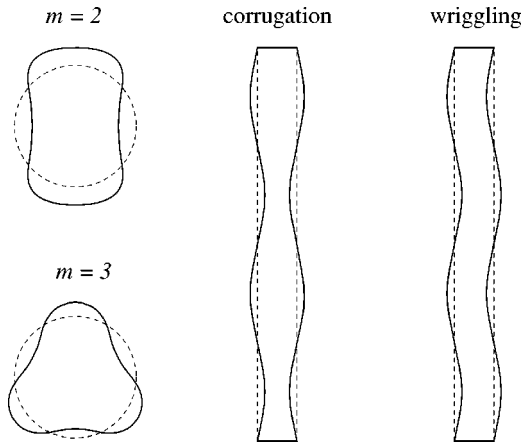

FIG. 3. Morphological instabilities of spots and stripes.

This result agrees with that of [18,28,47,58,62]. Let us point out that in one dimension Ren and Wei proved that the lamellar patterns of arbitrary periods are the only local minimizers of the free energy [47].

A comparison of the free energies per unit area of the lowest free energy hexagonal and lamellar patterns shows that the lamellar pattern has lower free energy when $f > 0.35$ [18]. For $0 < f < 0.35$ the hexagonal pattern has the lower free energy in two dimensions.

C. Morphological instabilities of solitary patterns

An important feature of patterns in systems with competing interactions is the fact that under certain conditions they can undergo *morphological instabilities* which lead to the distortions of their shapes and transitions between them [7]. In reaction-diffusion systems these instabilities have been analyzed in [2,45,48,50,51,53,57,63].

Apart from the arguments of Sec. III B, the physical reason for the existence of morphological instabilities is the fact that the energy of the long-range interaction increases faster than the area of the domain as its size gets bigger. Therefore, at some critical size it may become energetically favorable for the domain to split into two domains of smaller size or significantly change its shape. It is interesting to note that such an instability was first analyzed by Lord Rayleigh back in 1882 [64].

To investigate the morphological instabilities of the domain patterns in systems with long-range Coulomb interaction, we start by looking at the simplest possible patterns: spots and stripes. This analysis was performed in [50] in the context of reaction-diffusion equations of activator-inhibitor type. Here we will rederive these results using the interfacial approach [Eq. (42)].

1. Spot

Let us consider a single localized spot first. The fluctuations of the spot's shape are azimuthal distortions of its walls characterized by the azimuthal number m (Fig. 3). Because of the radial symmetry, the operator L in Eq. (42) is diagonal in the basis formed by the functions $e^{im\varphi}$, where φ is the polar angle that represents a point on the interface. For a spot of radius $\mathcal{R}_s \ll \epsilon^{-1}$ one can neglect screening and use G in the integral for $m > 0$, since these fluctuations do not change the overall area of the spot. Assuming $\rho = e^{im\varphi}$ and calculating the corresponding integrals, we obtain

$$\lambda = \lambda_0 + \frac{\sigma_0 m^2}{\mathcal{R}_s^2} + \frac{2\epsilon^2 \mathcal{R}_s}{m}, \tag{61}$$

where λ_0 is a constant that comes from the curvature and the $2(\hat{n}\cdot\vec{\nabla}\psi)$ term. In fact, we do not need to calculate this constant from the definition. Instead, we can use the translational symmetry of the problem and note that $\lambda = 0$ for $m = 1$ to find that

$$\lambda_0 = -\frac{\sigma_0}{\mathcal{R}_s^2} - 2\epsilon^2 \mathcal{R}_s . \tag{62}$$

Note that $\lambda_0 < 0$ and is responsible for the instability of the spot for large enough $\mathcal{R}_s$ (see also [2,51]).

According to Eq. (61), a single localized spot becomes unstable ($\lambda < 0$) with respect to the mth mode when $\mathcal{R}_s > \mathcal{R}_{cm}$, where

$$\mathcal{R}_{cm} = \left(\frac{\sigma_0 m(m+1)}{2\epsilon^2} \right)^{1/3}. \tag{63}$$

The instability is realized first with respect to the fluctuation with $m = 2$, so the spot is always unstable when $\mathcal{R}_s > \mathcal{R}_{c2}$, where

$$\mathcal{R}_{c2} = (3\sigma_0)^{1/3} \epsilon^{-2/3}. \tag{64}$$

The $m = 0$ case can be treated analogously; this leads once again to Eqs. (46) and (45). Therefore, comparing Eq. (64) with Eq. (49), we see that the spot can be stable only when

$$\delta_b < \delta < \delta_{c2}, \quad \delta_{c2} = 3^{-1/3} \kappa^2 \sigma_0^{2/3} \epsilon^{2/3} \ln \epsilon^{-1}, \tag{65}$$

so the spots are stable only in the limited range of $\delta \sim \epsilon^{2/3} \ll 1$ (apart from the logarithmic terms).

A similar analysis shows that the thin annulus of radius $\mathcal{R}_a \ll \epsilon^{-1}$ considered in Sec. IV A is always unstable with respect to the $m = 2$ wriggling mode, so we do not present this analysis in detail here.

2. Stripe

Let us now turn to the solitary stripe. Let us choose the reference frame in such a way that the stripe is oriented along the y axis in the zy plane. Because of the mirror symmetry of the stripe in the z direction, there are two basic types of fluctuation: the symmetric and the antisymmetric distortions of the stripe walls, both characterized by the transverse wave vector $k_\perp$ (Fig. 3). Because of the translational symmetry in the y direction the operator in Eq. (42) is diagonal in $k_\perp$. Assuming that $\rho^+ = e^{ik_\perp y}$ and $\rho^- = \pm\rho^+$, where $\rho^\pm$ are the positions of the right and left boundaries of the stripe, respectively, we can calculate the integral in Eq. (42) at the location of the right wall:

$$4\epsilon^2 \oint dS' G_\epsilon(x-x')\rho(x') = \frac{2\epsilon^2[1\pm\exp(-\mathcal{L}_s\sqrt{\epsilon^2\kappa^2+k_\perp^2})]}{\sqrt{\epsilon^2\kappa^2+k_\perp^2}} e^{ik_\perp y}, \quad (66)$$

where "+" corresponds to the symmetric and "−" to the antisymmetric fluctuations; $\mathcal{L}_s$ is the width of the stripe.

For the stripe, the curvature terms in Eq. (42) are zero, and the $2(\hat{n}\cdot\vec{\nabla}\psi)$ term reduces to a constant $\lambda_0<0$. The case of the symmetric and antisymmetric fluctuations must be treated separately. For $k_\perp \gg \epsilon$ the expression for $\lambda=\lambda_+$ for the symmetric fluctuation is (to leading order in ϵ)

$$\lambda_+ = \lambda_0 + \sigma_0 k_\perp^2 + \frac{2\epsilon^2[1+\exp(-k_\perp\mathcal{L}_s)]}{k_\perp}. \quad (67)$$

On the other hand, when $\mathcal{L}_s \ll \epsilon^{-1}$ and $k_\perp\mathcal{L}_s \ll 1$, to leading order in ϵ the expression for $\lambda=\lambda_-$ for the antisymmetric fluctuation becomes

$$\lambda_- = \lambda_0 + \sigma_0 k_\perp^2 + 2\epsilon^2\mathcal{L}_s - \epsilon^2\mathcal{L}_s^2\sqrt{\epsilon^2\kappa^2+k_\perp^2}. \quad (68)$$

Once again, we can use translational symmetry in the z direction to calculate λ_0, since $\lambda_-=0$ when $k_\perp=0$. We get

$$\lambda_0 = -2\epsilon^2\mathcal{L}_s + \epsilon^3\kappa\mathcal{L}_s^2 + O(\epsilon^4\mathcal{L}^3). \quad (69)$$

The analysis of the transcendent Eq. (67) with λ_0 given by the first term in Eq. (69) shows that the instability of the stripe with respect to symmetric distortions of its walls (corrugation) with $k_\perp=k_c$ occurs at $\mathcal{L}_s>\mathcal{L}_{c1}$, where [50]

$$k_c = 1.13\sigma_0^{-1/3}\epsilon^{2/3}, \quad \mathcal{L}_{c1} = 1.66\sigma_0^{1/3}\epsilon^{-2/3}. \quad (70)$$

According to Eq. (68), the stripe becomes unstable with respect to antisymmetric distortions of its walls (wriggling) at $k\to 0$ and $\mathcal{L}_s>\mathcal{L}_{c2}$, where

$$\mathcal{L}_{c2} = (2\sigma_0\kappa)^{1/2}\epsilon^{-1/2}. \quad (71)$$

This is also clear from Eq. (53). Comparing Eqs. (71) and (70), one can see that the instability with respect to wriggling is realized before the instability with respect to corrugation. In view of Eq. (55), the stripe is stable only when

$$\epsilon\ln\epsilon^{-1} \lesssim \delta < \delta_\perp, \quad (72)$$

where $\delta_\perp$ is defined in Eq. (54). Thus, the region of existence of stable stripes is wider than that for spots [see Eq. (65)].

D. Morphological instabilities of hexagonal and lamellar patterns

The solution of Eq. (42) in the case of an arbitrary multidomain pattern is a formidable task. However, a simplification of this problem is possible in the case of periodic patterns. Then, by Bloch theorem, the operator L can be partially diagonalized by considering the fluctuations modulated by the wave vector $\mathbf{k}$ which lies in the first Brillouin zone of the underlying domain lattice. The situation here is not unlike the problem of finding the band structure of a crystal [61]. Below, we consider the stability of hexagonal and lamellar patterns in two dimensions.

1. Hexagonal pattern

Let us consider a hexagonal pattern of period $\mathcal{L}_p$ made of circular domains of radius $\mathcal{R}_s$. For each domain centered at $\mathbf{R}_n$ let us write the displacement ρ_n as

$$\rho_n(\varphi) = \sum_m a_m e^{i\mathbf{k}\cdot\mathbf{R}_n - im\varphi}, \quad (73)$$

where the angle φ represents a point on the interface of each domain. Equation (42) for fluctuations with a given $\mathbf{k}$ in the first Brillouin zone then reduces to

$$\left(\frac{\sigma_0 m^2}{\mathcal{R}_s^2} + \lambda_0 - \lambda\right) a_m = -\sum_{m'} \mathsf{R}_{mm'}(\mathbf{k}) a_{m'}, \quad (74)$$

where m and m' are the azimuthal numbers, λ_0 is a constant independent of m and $\mathbf{k}$ (assuming that with good accuracy $\hat{n}\cdot\vec{\nabla}\psi$ is radially symmetric in the interface), and $\mathsf{R}_{mm'}(\mathbf{k})$ are the $\mathbf{k}$-dependent matrix elements of $4\epsilon^2 G_\epsilon(x-x')$. The calculation in Appendix C 1 shows that [48]

$$\mathsf{R}_{mm'}(\mathbf{k}) = \frac{16\pi\epsilon^2\mathcal{R}_s}{\mathcal{L}_p^2\sqrt{3}} \sum_n \frac{e^{i(m-m')(\vartheta_{\mathbf{k}+\mathbf{k}_n}+\pi/2)}}{|\mathbf{k}+\mathbf{k}_n|^2+\epsilon^2\kappa^2} \times J_m(|\mathbf{k}+\mathbf{k}_n|\mathcal{R}_s) J_{m'}(|\mathbf{k}+\mathbf{k}_n|\mathcal{R}_s), \quad (75)$$

where $\mathbf{k}_n$ run over the reciprocal lattice, $J_m(x)$ are Bessel functions of the first kind, and $\vartheta_{\mathbf{k}+\mathbf{k}_n}$ is the angle between the vector $\mathbf{k}+\mathbf{k}_n$ and the x axis.

The value of λ_0 can be calculated by noting that the translational invariance of the system requires that $\lambda=0$ for $\mathbf{k}=\mathbf{0}$ and $m=1$, so (Appendix C 1)

$$\lambda_0 = -\frac{\sigma_0}{\mathcal{R}_s^2} - 2\epsilon^2\mathcal{R}_s\left(1 - \frac{2\pi\mathcal{R}_s^2}{\sqrt{3}\mathcal{L}_p^2}\right). \quad (76)$$

In writing the above equations we assumed that $\mathcal{R}_s \sim \mathcal{L}_p \ll \epsilon^{-1}$.

As was shown qualitatively by Kerner and Osipov, for the most dangerous fluctuations the wave vector $\mathbf{k}$ will lie close to the edge of the Brillouin zone [2]. There are two basic types of fluctuations we need to consider: fluctuations that lead to repumping of the order parameter between neighboring domains [Fig. 4(a)] and fluctuations that lead to asymmetric distortions of the domains [Fig. 4(b)] ([2]; see also Sec. III B). Analysis of Eq. (74) shows that the most dangerous fluctuations leading to repumping have $\mathbf{k}=\frac{1}{3}(\mathbf{b}_1-\mathbf{b}_2)$, where $\mathbf{b}_1$ and $\mathbf{b}_2$ are reciprocal lattice vectors that make a 120^o angle (see Appendix C 1), while the most dangerous fluctuations leading to distortions have $\mathbf{k}=\frac{1}{2}(\mathbf{b}_1+\mathbf{b}_2)$ [48]. The instability $\lambda<0$ occurs with respect to repumping when $\mathcal{L}_p<\mathcal{L}_{p0}$ or with respect to the asymmetric distortion when $\mathcal{L}_p>\mathcal{L}_{p2}$, where $\mathcal{L}_{p0,2}$ depend on ϵ and $\mathcal{R}_s/\mathcal{L}_p$. The resulting stability diagram obtained by numerical solution of Eq.

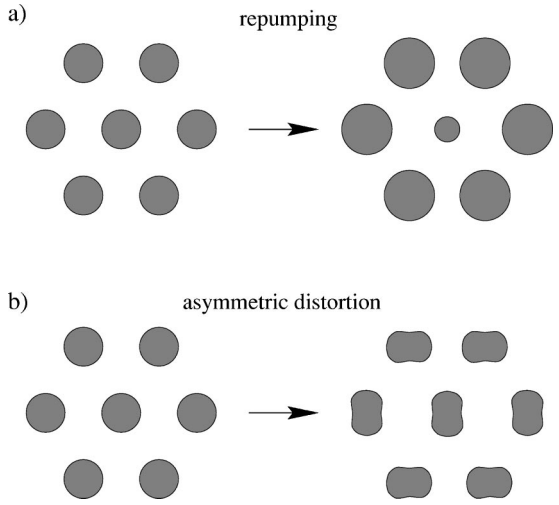

FIG. 4. Two major types of instabilities of the hexagonal pattern.

(74) with the parameters of the mean-field model from Sec. II B is presented in Fig. 5. From this figure one can see that only the patterns with period $\mathcal{L}_{p0}<\mathcal{L}_p<\mathcal{L}_{p2}$ are stable.

Figure 5 also shows the period of the lowest free energy hexagonal pattern given by Eq. (58). One can see that this pattern is stable for all values of $\mathcal{R}_s/\mathcal{L}_p$ (except, possibly, for $\mathcal{R}_s/\mathcal{L}_p$ close to 0.5 where the assumption about the circular shape of the domains ceases to be valid). As was noted in Sec. IV B, in two dimensions the lowest free energy hexagonal pattern is expected to be the global minimizer of the free energy if $f<0.35$, or, equivalently, if $\mathcal{R}_s/\mathcal{L}_p<0.31$, whereas for $0.31<\mathcal{R}_s/\mathcal{L}_p<0.37$ (the second condition means that $\overline{\phi}<0$) the global minimizer should be the lamellar pattern. Figure 5, however, does not show the transition from the hexagonal to the lamellar pattern, so in fact the lowest-energy hexagonal pattern is at least *metastable* for all values of $\overline{\phi}$ at which it exists.

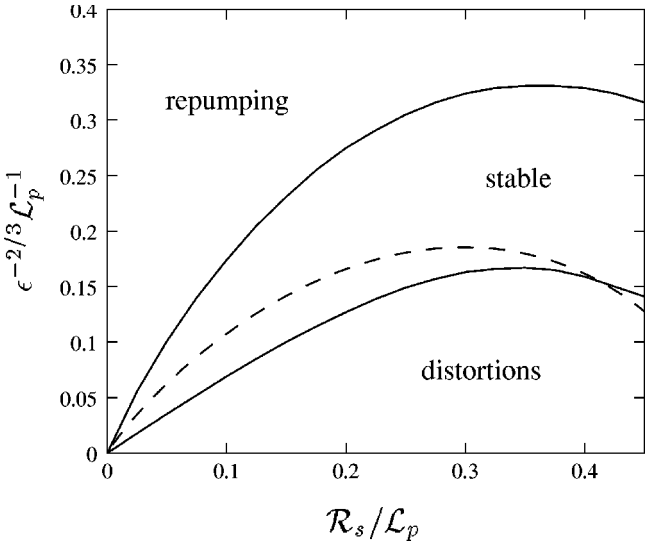

FIG. 5. The stability diagram for the hexagonal pattern with $\sigma_0=2\sqrt{2}/3$. The dashed line corresponds to the hexagonal pattern with the lowest free energy given by Eq. (58).

2. Lamellar pattern

In the case of the lamellar pattern one should consider fluctuations that are modulated by the wave vector $k_\parallel$ from the first Brillouin zone in the direction along the normal to the stripes and an arbitrary wave vector $k_\perp$ in the transverse direction:

$$\rho_n^{\pm}=\rho_0^{\pm}e^{ik_\perp y+ik_\parallel n\mathcal{L}_p}, \tag{77}$$

where $\rho_n^{\pm}$ are the displacements of the right and left walls of the stripe in the nth period of the lamellar pattern at $y=0$. Because of the translational symmetry in the direction along the stripes, these fluctuations are eigenfunction of L in Eq. (42). One can then reduce the operator L to a 2×2 matrix, so after a tedious calculation (Appendix C 2; see also [2,63])

$$\lambda_{\pm}=\lambda_0+\sigma_0k_\perp^2+\mathsf{R}_{\pm}(k_\parallel,k_\perp), \tag{78}$$

where $\mathsf{R}_{\pm}(k_\parallel,k_\perp)$ are given by

$$\begin{aligned}\mathsf{R}_{\pm}(k_\parallel,k_\perp)=&\frac{4\epsilon^2e^{k\mathcal{L}_p}}{k(1-2e^{k\mathcal{L}_p}\cos k_\parallel\mathcal{L}_p+e^{2k\mathcal{L}_p})}\\&\times[\sinh k\mathcal{L}_p\pm(\{\sinh[k(\mathcal{L}_p-\mathcal{L}_s)]\\&+\cos k_\parallel\mathcal{L}_p\sinh k\mathcal{L}_s\}^2+\sin^2k_\parallel\mathcal{L}_p\sinh^2k\mathcal{L}_s)^{1/2}],\end{aligned} \tag{79}$$

where $k=\sqrt{\epsilon^2\kappa^2+k_\perp^2}$. As before, the value of λ_0 is determined with the aid of the translational invariance of the system, which requires that $\lambda=0$ for $k_\parallel=k_\perp=0$ for the antisymmetric fluctuation. This gives the following value of λ_0 (to leading order in ϵ):

$$\lambda_0=-2\epsilon^2\mathcal{L}_s\left(1-\frac{\mathcal{L}_s}{\mathcal{L}_p}\right). \tag{80}$$

The analysis of Eq. (78) shows that [in the validity range of Eq. (79), that is, when $\mathcal{L}_p\gg\ln\epsilon^{-1}$; see also [2]] the repumping instability is not realized for the lamellar pattern. This can be explained by a simple argument: the curvature of the stripes is equal to zero, so there is no force that would lead to domain collapse as in the case of the spot. The analysis of Eq. (78) also shows that the most dangerous fluctuation leads to antisymmetric distortions of the stripe and has $k_\parallel=0$ and $k_\perp\to0$ (see also [63,65]). All other instabilities, such as the corrugation instability, occur at higher values of $\mathcal{L}_p\sim\epsilon^{-2/3}$ (compare with [66,67]). Also notice that when $k_\perp=0$, which corresponds to the one-dimensional situation, the lamellar pattern is always stable when $\ln\epsilon^{-1}\ll\mathcal{L}_p\ll\epsilon^{-1}$ (see Appendix C 2). This is in agreement with the result of Ren and Wei that in this situation the lamellar patterns are all local minimizers of Eq. (29) [47].

Solving Eq. (78) with $k_\parallel=0$, we obtain that the instability is realized when $\mathcal{L}_p=\mathcal{L}_p^*$, where $\mathcal{L}_p^*$ is the period of the lowest-free-energy lamellar pattern given by Eq. (60) (see Appendix C 2). This result was also obtained by Yeung and Desai in the case $f=0.5$ [28]. Thus, the lowest-free-energy lamellar pattern is *marginally* stable with respect to the wrig-

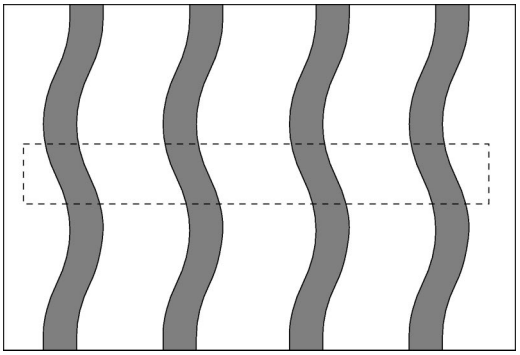

FIG. 6. Wriggled lamellar pattern.

gling instability. This fact has a simple geometric interpretation, and should in fact be true for any system with long-range competing interactions. Indeed, consider a small wriggling modulation of the lamellar pattern (Fig. 6). Inside the dashed rectangle the stripes can be considered as straight, but rotated by a small angle ϑ. This pattern can be again considered as a lamella, but with a smaller period $\mathcal{L}_p' = \mathcal{L}_p \cos\vartheta$. The free energy of the system in this case will increase if $\mathcal{L}_p < \mathcal{L}_p^*$, since the free energy is a decreasing function of $\mathcal{L}_p$ for these values of $\mathcal{L}_p$, or decrease if $\mathcal{L}_p > \mathcal{L}_p^*$, since there the free energy is an increasing function of $\mathcal{L}_p$. The case $\mathcal{L}_p = \mathcal{L}_p^*$ is marginal. Therefore, the lamellar pattern will be unstable with respect to wriggling if $\mathcal{L}_p > \mathcal{L}_p^*$, or stable otherwise.

It is interesting to note the analogy between the lamellar patterns and smectic-A phases. In smectics the long-wave modulations of the layered structure cost free energy $\Delta F \propto (\bar{B} k_\parallel^2 + K_1 k_\perp^4) |u_z(k_\parallel, k_\perp)|^2$, where $u_z(k_\parallel, k_\perp)$ is the amplitude of the layer displacements modulated by wave vectors $k_\parallel$ and $k_\perp$ along and perpendicular to the layers, respectively [42,68]. This is precisely what we get for the pattern with $\mathcal{L}_p = \mathcal{L}_p^*$ in the limit of small $k_\parallel, k_\perp$ (see Appendix C 2). Furthermore, in view of this analogy the long-wave instability of lamellar patterns with $\mathcal{L}_p > \mathcal{L}_p^*$ is equivalent to the Helfrich-Hurault instability of smectics under stretching deformations. Also note that under the influence of thermal fluctuations the lamellar pattern with $\mathcal{L}_p = \mathcal{L}_p^*$ is subject to the Landau-Peierls instability [42,68]. We would like to point out, however, that all this does not apply to metastable lamellar patterns with $\mathcal{L}_p < \mathcal{L}_p^*$, which, according to our calculations, have finite shear modulus.

V. SCENARIOS OF DOMAIN PATTERN FORMATION

The analysis in the preceding sections shows that patterns in systems with long-range Coulomb interactions are very sensitive to the parameters $\bar{\phi}$ and ϵ and can undergo various instabilities. As the temperature is lowered, both ϵ and $|\bar{\phi}|$ rapidly decrease; see, for example, Eqs. (7) and (6). In this situation a small variation of the temperature may trigger complex spatiotemporal behavior in the system. Now we would like to ask the following questions: How do patterns form in an initially homogeneous system and how do the patterns already present in the system react to changes in the external parameters? In principle, to answer these questions we need to specify the dynamics of patterns. This question is quite complicated and significantly depends on the particular system, despite the universality possessed by the free energy (for various examples, see [2,28,37,69]). However, if the dynamics of the system is *dissipative*, it will result in a decrease of the free energy of the patterns with time. Note that since the free energy functionals in Eqs. (5) and (29) are bounded from below in systems of finite volume, in the absence of noise the patterns must evolve to local minimizers of the free energy. To mimic this behavior, we will use the simple gradient descent dynamics defined by

$$\frac{\partial \phi}{\partial t} = -\frac{\delta F}{\delta \phi}, \tag{81}$$

where F is given by Eq. (5). This evolution equation is, in fact, applicable to a number of systems with nonconserved order parameter [1,2,4,27,34]. However, our conclusions should not qualitatively depend on this particular choice, since the evolution of patterns will generally be guided by the free energy landscape and the morphological instabilities of the patterns. Note that Eq. (81) is equivalent to a reaction-diffusion system with a fast inhibitor and can be reduced to a free boundary problem in the limit $\epsilon \to 0$ [56], which, in turn, is the gradient descent dynamics for the interfacial free energy [45].

A. Nucleation

The first question is how the domain patterns form in the system in the first place. As was discussed in Sec. II B, at sufficiently high temperatures above T_c the homogeneous phase is the only equilibrium state. In the mean-field model of Sec. II B the homogeneous phase becomes unstable as the temperature of the system is lowered. At $\bar{\phi} = 0$ this happens when $\epsilon(\tau) = \epsilon_c \sim 1$. On the other hand, when the original (unscaled) value of $\bar{\phi}$ is different from 0, the homogeneous state will remain stable even for lower temperatures. The greater the (unscaled) value of $|\bar{\phi}|$, the lower the temperature at which the homogeneous phase will lose its stability. This means that for $\alpha \ll 1$ the homogeneous phase will typically remain stable in a range of τ for which $\epsilon \ll 1$.

On the other hand, as was shown in Sec. IV A, when the scaled value of $|\bar{\phi}|$ is less than $|\bar{\phi}_b| = 1 - \delta_b$, in addition to the stable homogeneous phase the system can support stable domain patterns (spots). In a narrow range of $|\bar{\phi}_m| < |\bar{\phi}| < |\bar{\phi}_b|$, where $|\bar{\phi}_m| = 1 - \delta_m$, the spots will be energetically unfavorable. On the other hand, in a wide range of $|\bar{\phi}| < |\bar{\phi}_m|$ the domain patterns will have lower free energy than the homogeneous phase. In the mean-field model of Sec. II B the homogeneous phase remains stable as long as $|\bar{\phi}| > |\bar{\phi}_c| \simeq 1/\sqrt{3}$ for $\epsilon \ll 1$. Therefore, at $|\bar{\phi}_c| < |\bar{\phi}| < |\bar{\phi}_m|$ the homogeneous phase is *metastable*.

The metastability of the homogeneous phase implies the possibility of *nucleation* of the domain patterns as a result of

thermal fluctuations. It is natural to assume that the nucleating droplet in two dimensions is a spot (it is localized in space and radially symmetric). Let us consider the nucleation of positive domains from a negative homogeneous phase. In this case the value of $\bar{\phi}$ is negative, so, as the temperature of the system decreases, the value of $\bar{\phi}$, as well as δ [recall Eq. (44)], increases. As was shown in Sec. IV A, at $\delta > \delta_b$ there are two spot solutions. The spot with radius $\mathcal{R}=\mathcal{R}_n$ is in unstable equilibrium with the homogeneous phase (see Fig. 1). Therefore, it is this solution that should play the role of the nucleation droplet in our system. Note that the radius of the nucleation droplet $\mathcal{R}_n < \mathcal{R}_{\min}$ and is bounded for all δ, in contrast to systems with first-order phase transitions. This is a distinctive property of systems with long-range Coulomb interactions.

According to Eq. (43), for δ close to δ_b the free energy cost of the nucleation droplet is (apart from a weak logarithmic dependence)

$$\Delta F_{\text{drop}} \propto \epsilon^{-2/3} \gg 1. \tag{82}$$

Note that in three dimensions the same arguments give $\Delta F_{\text{drop}} \propto \epsilon^{-4/3} \gg 1$ also. Since this free energy barrier is high, the arguments of nucleation theory apply here.

In the narrow range of $\delta_b < \delta < \delta_m$, a nucleation event will result in the formation of a stable spot whose free energy is higher than that of the homogeneous phase. Therefore, in this situation the spot itself will be metastable and will decay back into the homogeneous phase. However, when δ is not in the immediate vicinity of δ_b, the free energy barrier the spot has to overcome to decay will also scale as in Eq. (82), so such spots will be long-lived metastable states that can be excited by thermal fluctuations. Therefore, the thermodynamic equilibrium state of the system for these parameters is a rarefied gas of noninteracting spots. In this situation the spots will play the role of *quasiparticles*.

When δ exceeds δ_m, the spot becomes thermodynamically more favorable than the homogeneous phase. For $\delta_m < \delta < \delta_{c2}$ the spots with radius $\mathcal{R}_s$ are stable, so a nucleation event will result in the formation of a single stable spot. This is another distinctive feature of nucleation in our system: sufficiently close to δ_b a single nucleation event will result in the formation of only one spot. However, in order for the system to come to the equilibrium, it has to become filled with spots, so the transition from the metastable homogeneous phase to the equilibrium multidomain pattern requires many nucleation events. These events will occur on an extremely long time scale $\tau_{\text{nucl}} \sim e^{c\Delta F_{\text{drop}}} \gg \tau_{\text{rel}}$, where $c \gtrsim 1$ is a constant and τ_{rel} is the characteristic system relaxation time. Dynamically, this phenomenon can be identified as *aging* [70].

According to Eq. (49), as the temperature decreases, and therefore $\bar{\phi}$ and δ increase, the radius of the nucleation droplet gets smaller (in scaled units), while the radius of the stable spot becomes larger, so at $\delta = \delta_{c2}$ the spot with radius $\mathcal{R}_s$ will become unstable with respect to the morphological instability (see Sec. IV C). In this case the nucleation scenario will change. Instead of a single spot, a more complex pattern will form as a result of a single nucleation event (see Sec. V B). At the same time, the nucleation barrier decreases with temperature. At $\delta \sim 1$ the free energy barrier becomes $\Delta F_{\text{drop}} \sim 1$ [see Eqs. (43) and (49)]. So in the renormalized model of Sec. II D nucleation becomes meaningless for these values of δ, and one can talk about the *instability* of the homogeneous phase. Let us point out that for $\delta \gtrsim \delta_{c2}$ the annulus should also be considered as a potential candidate for the nucleation droplet. Comparison of the free energies of an annulus and a spot of radius $\mathcal{R}_n$ shows, however, that the spot always has lower free energy.

Let us consider nucleation in the renormalized model of Sec. II D in more detail. Depending on the cooling rate, several situations are possible. When the cooling rate is very small (with the characteristic time scale much longer than τ_{nucl}), the system will have enough time to equilibrate and will get filled with spots. If the cooling rate is such that its characteristic time scale is comparable to τ_{nucl}, the system will enter into the aging regime. Notice that these phenomena will occur only in a narrow range of temperatures at which $\delta \sim \delta_b$.

The situation will change qualitatively when $\delta > \delta_{c2}$, when the temperature falls below the value at which the spot becomes unstable with respect to a morphological instability. In this case a single nucleation event will produce a spot which will further develop into a more complex extended pattern, filling up the whole system (see Sec. V B). The time scale of this process is τ_{rel} and is much shorter than τ_{nucl}, so, if the cooling rate is sufficiently fast, only a single nucleation event is enough to create a pattern that will fill the entire system. This will also be the case in the mean-field model of Sec. II B. Finally, if the cooling rate is very fast, the system will not have enough time to nucleate even a single domain, so it will enter the region in which the homogeneous state of the system is unstable. In that case a pattern consisting of domains whose characteristic size is comparable with the correlation length will form spontaneously and then evolve toward equilibrium via coarsening (see Sec. V C).

If small local inhomogeneities exist in the system, they can work as nucleation centers. One could, for example, have a slightly nonuniform distribution of $\bar{\phi}$ across the system. If their amplitude and size are not very large, the nucleation events will produce stable spots that will be pinned to the locations of these inhomogeneities. If, on the other hand, the amplitude and size of these inhomogeneities are large enough, the spots that nucleate at their locations may be unstable with respect to the morphological instabilities, so they can work as nucleation centers for spatially extended patterns.

B. Growth of complex patterns

As was discussed in Sec. V A, typically a spot that forms as a result of a nucleation event will be unstable with respect to deformations of its shape. After such a spot is formed, it will start to grow into a more complex pattern on the time scale of $\tau_{\text{rel}} \ll \tau_{\text{nucl}}$. Therefore, in the process of growth of such a spot thermal fluctuations become unimportant. A typical evolution of a pattern in this situation is shown in Fig. 7,

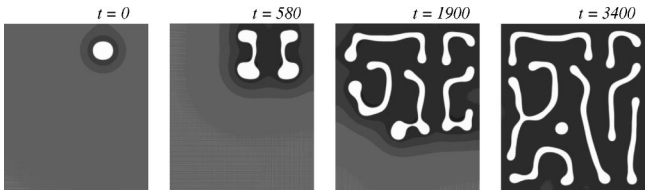

FIG. 7. Formation of a complex pattern as the result of instability of a spot. Results of the numerical solution of Eq. (81) with $\epsilon = 0.025$ and $\bar{\phi} = -0.6$, with no-flux boundary conditions. The system is 400×460.

which shows the result of the numerical solution of Eq. (81) in this parameter regime. At long times, the system evolves to a disordered metastable equilibrium pattern.

The evolution of unstable localized patterns within the framework of Eq. (81) and the corresponding interfacial dynamics problem was studied in detail in [45,56,57]. The solution of the interfacial dynamics equation shows that for sufficiently large δ the morphological instability of a spot will always lead to self-replication of spots [56]. As a result of the instability, the spot grows more and more distorted, until at some point the interfaces touch, what leads to the pinch-off and splitting (fission) of one domain into two. The daughter domains move away from each other, and the process of splitting repeats itself. This self-replication process will continue until the whole system is filled with the multidomain pattern [56,57].

Note that these results hold in the asymptotic limit $\epsilon \to 0$, in which $\mathcal{R}_s \sim \epsilon^{-2/3} \ll \epsilon^{-1}$, so the screening effects may be ignored. On the other hand, for reasonably small but finite ϵ the effective interaction may get truncated at distances comparable to the sizes of the spots. In particular, as the spots move away from each other after splitting, the interaction between the distant portions of their interfaces may get screened, so the spots will remain connected by a *stripe* as they move apart (see Fig. 7, $t = 580$). For $\delta_{c2} < \delta \lesssim \delta_{c3}$ (the latter corresponds to the value of δ at which the spot becomes unstable with respect to the $m = 3$ mode) the tips on both sides of the stripe will be stable, so as a result of the destabilization a spot will transform into a stripe spanning the system. Note that according to Eq. (53), this can happen only when $\delta > \delta_\perp$, when the stripe is energetically favorable. According to Eqs. (54) and (65), for not very small values of ϵ it may be possible to have $\delta_{c2} \sim \delta_\perp$. Note that for these values of δ the newly grown stripe will destabilize with respect to wriggling and fill up the entire space of the system. Furthermore, the stripe segments with the highest curvature may become unstable with respect to fingering [57]. This is what we see in the numerical simulations of Eq. (81) in this parameter range. When $\delta \gtrsim \delta_{c3}$, the tips of a stripe growing as a result of a splitting event can further destabilize with respect to the $m = 3$ mode, which will result in tip splitting and the formation of a *labyrinthine* pattern. Note that similar results were obtained in the case of reaction-diffusion systems with weak activator-inhibitor coupling [45].

From the arguments above it is possible to conclude that, following a nucleation event at δ not very far from δ_{c2} and for not very small values of ϵ, the dominating pattern morphology is that of the stripe. Nevertheless, for larger values of δ the spot morphology starts to compete with the stripe morphology. This is because for large δ interfaces will tend to split, so the forming labyrinthine pattern will become *disconnected* [57]. When the value of ϵ is decreased, one should find coexistence of both spot and stripe morphologies in the patterns formed as a result of the destabilization of a spot (Fig. 7). So all the processes associated with the dynamics of the interfaces, fission, elongation, tip splitting, fingering, and wriggling [7], should generally be important for the evolution of a single unstable spot.

C. Coarsening and disorder

If the system is quenched deeply into the region in which the homogeneous phase is unstable, at first a small-scale multidomain pattern will form. Since the effect of the long-range interaction can be seen only on the length scale $R \gtrsim \epsilon^{-2/3}$, initially the long-range interaction will be negligible. Therefore, immediately following the quench the pattern will undergo transient *coarsening*. Note that in systems with nonconserved order parameter this transient coarsening may proceed at arbitrary $\bar{\phi}$, since the long-range interaction ensures the conservation of the total amount of the order parameter. For example, in the case of Eq. (81) the interfaces of the domains will be driven by curvature subject to global coupling, so the characteristic radius of the domains will obey the standard $t^{1/2}$ law independently of the volume fraction [37,71,72]. As a result, the characteristic size of the domains will grow until it becomes comparable with the equilibrium size of Eq. (14). Then the long-range interaction will stabilize the pattern, so at some point the coarsening will become *arrested* (see also [26,73]). This scenario is observed in experiments on thin diblock copolymer films [74]. Note that this coarsening can be viewed as a consequence of the repumping instability discussed in Secs. III B and IV D.

When the temperature in the mean-field model from Sec. II B is slowly lowered, so that the value of $|\bar{\phi}|$ becomes lower than $|\bar{\phi}_c|$, the homogeneous state becomes unstable with respect to fluctuations with wavelength $\lambda \sim \epsilon^{-1/2}$ (see Sec. II B). Thus, at the threshold of the instability domain pattern with characteristic size $\sim \lambda$ will start to form [2,57]. These domains will still be smaller than the equilibrium size $R \sim \epsilon^{-2/3}$, so the instability will be followed by coarsening, just as in the case of the renormalized model and in the mean-field model not close to $\bar{\phi}_c$.

The results of the simulations of Eq. (81) displaying transient coarsening are presented in Fig. 8. In all these simulations the initial conditions were taken as $\phi = \bar{\phi}$ plus small random noise. One can see that the morphology of the pattern is determined by the volume fraction of the positive domains. When $\bar{\phi} = 0$ the pattern that forms at the end of the simulation is a bicontinuous domain pattern similar to patterns forming in the process of Ostwald ripening after the critical quench [41]. When there is a small asymmetry between the positive and negative domains [Fig. 8(b)], the pattern at the end of the simulation looks like a collection of disconnected spots and stripes of different shapes and sizes.

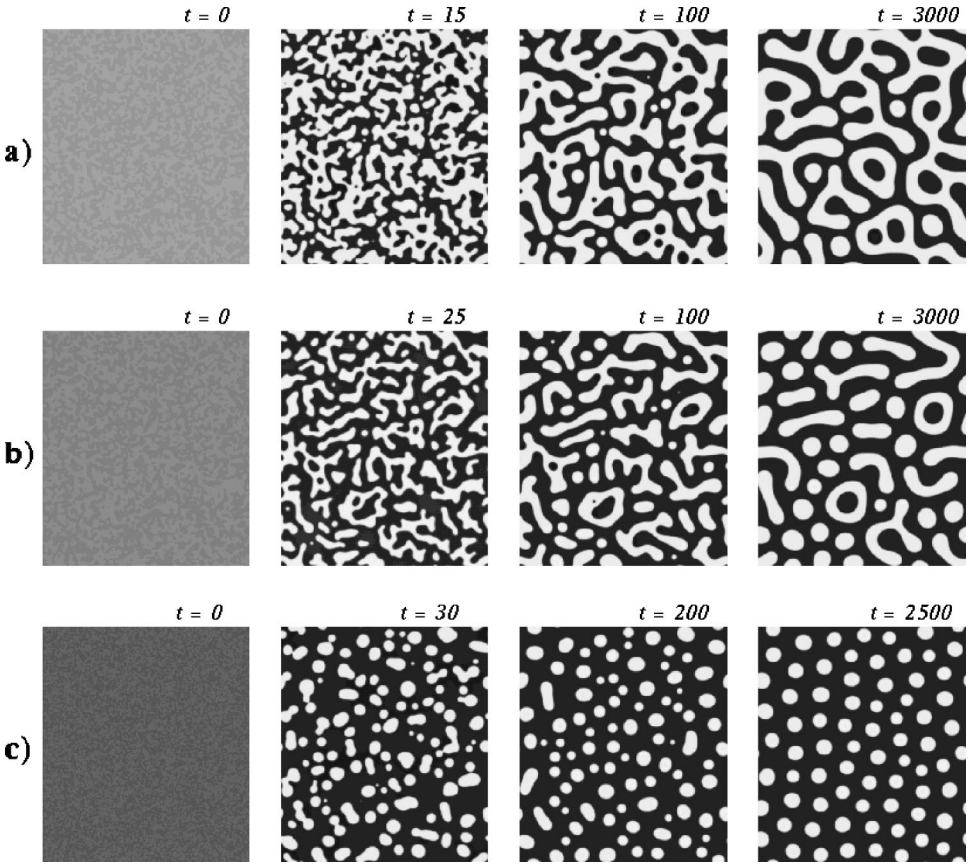

FIG. 8. Coarsening of the domain patterns at different values of $\bar{\phi}$: $\bar{\phi}=0$ (a), $\bar{\phi}=-0.2$ (b), $\bar{\phi}=-0.5$ (c). Results of the numerical simulations of Eq. (81) with $\epsilon=0.025$ and periodic boundary conditions. The system is 400×460.

When the asymmetry between the positive and negative domains is strong [Fig. 8(c)], only the spot morphology survives, and in the end the pattern is made of a polydisperse mixture of spots.

Let us emphasize that the patterns that form at the end of the simulations of Fig. 8 do not change in time, that is, they are metastable. Each of these patterns is completely disordered, and is *in no way* close to the perfectly ordered patterns that are expected to be the global minimizers of the free energy. In the absence of noise the shape of the pattern at long times is determined only by the random initial conditions. Numerical analysis of Eq. (81) shows that by changing the random seed which determines the initial condition at the start of the simulation one will get totally different metastable patterns in the end, so the system is in fact very sensitive to the initial conditions. This also suggests that, in addition to the ordered equilibrium patterns, there exist a huge number of irregular metastable patterns which locally minimize the free energy. Thus, a typical pattern that should form as a result of a fast quench must be disordered.

Once metastable equilibrium is achieved, the patterns will evolve by thermally activated processes. Indeed, in order for a pattern with lower free energy to form, some of the domains may have to disappear and some may have to be created, since the topology of different metastable domain patterns is not generally the same. This requires overcoming large free energy barriers $\Delta F\propto\epsilon^{-2/3}$. Once again, on the time scale $\tau_{\mathrm{nucl}}\sim e^{c\Delta F}$ the system will enter the aging regime. To mimic this situation, we performed a numerical simulation of Eq. (81) with a special initial condition in the form of a metastable hexagonal pattern with a single bigger spot in the center (Fig. 9). As time goes on, the pattern tries to adjust to accommodate a defect it is presented with. Let us emphasize that, according to Fig. 9, the defect *propagates* to distances much larger than the characteristic size of the domains. In the end, the pattern becomes completely

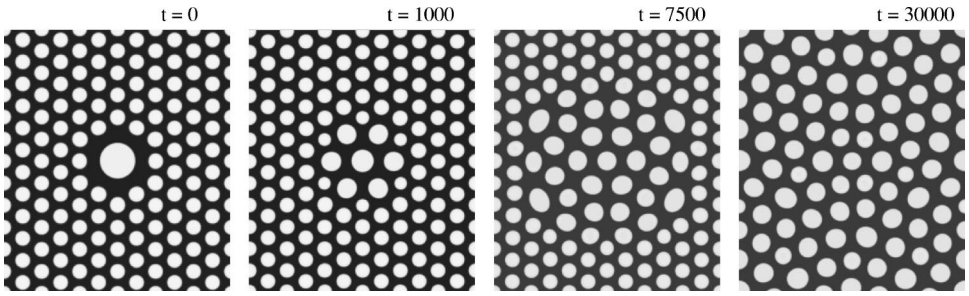

FIG. 9. The effect of a large-scale fluctuation on a hexagonal pattern. Result of the numerical solution of Eq. (81) with $\epsilon=0.025$, $\bar{\phi}=-0.2$, and periodic boundary conditions. The system is 400×460.

disordered, with no traces of the original hexagonal ordering.

Let us now ask a different question. Suppose that we already have an equilibrium domain pattern in the system. What happens if at some moment the temperature of the system is raised or lowered? This question is related to what happens if the system is gradually cooled below the transition temperature. Suppose the system is initially occupied by the lowest-energy hexagonal pattern (at a given temperature). When the temperature of the system is lowered, the values of ϵ and $|\overline{\phi}|$ will decrease, so this pattern will no longer correspond to the equilibrium pattern. To see this, let us write down the length scales in Eq. (16) in the original (unscaled) variables. Using the mean-field scaling [42] and the definition of ϵ from Eq. (6), for example, we obtain

$$l \sim |\tau|^{-1/2}, \quad \lambda \sim \alpha^{-1/4},$$

$$R \sim \alpha^{-1/3}|\tau|^{1/6}, \quad L \sim \alpha^{-1/2}|\tau|^{1/2}. \tag{83}$$

One can see from here that if the temperature is abruptly lowered the equilibrium size R will increase. At the same time, the *physical* size of the pattern will remain the same, so the relative size of the pattern will decrease with respect to the new value of R.

If the temperature drop is sufficiently small, the pattern will remain metastable (see Sec. IV D). However, when the temperature falls below a certain critical temperature, the pattern will become *unstable* with respect to repumping (Sec. IV D). The repumping will lead to the collapse of a fraction of the domains and growth of the rest, so effectively this will be equivalent to an increase of the characteristic interdomain distance. The resulting pattern will again be metastable. Note, however, that it will necessarily become disordered, since randomness is involved in the destabilization of the hexagonal pattern. When the temperature gets lower, the metastable pattern will again destabilize, and produce a new metastable pattern with a greater characteristic domain size. This process will go on. Thus we will have a stepwise relaxation process creating disordered patterns. A similar effect will be realized if one takes a hexagonal pattern as the initial condition and gradually raises the temperature. At some moment the pattern will become unstable with respect to the asymmetric deformations, so domains of complex shapes will start to form, thus effectively making the distance between the patterns smaller. Such a metastable domain pattern will further destabilize at higher temperature. These conclusions are confirmed by numerical simulations of Eq. (81) [48]. Note that these arguments imply that disordered patterns will form even as a result of a slow (but fast compared to τ_{nucl}) quench below the transition temperature. All this indicates that disorder is an intrinsic state of the systems with long-range competing interactions. This is also seen in experiments [7,74–76].

Similarly, when one starts with a lamellar pattern and raises the temperature, the pattern will become unstable with respect to wriggling (see Sec. IV D). If the temperature is further increased, corrugation instability and fingering will follow. Notice that, in contrast to hexagonal patterns, the lamellar pattern will always remain metastable when the temperature is lowered, since there is no repumping instability in this case. This means that a metastable lamellar pattern is more likely to survive after a slow (but fast compared with τ_{nucl}) critical quench.

VI. CONCLUSIONS

In this work we have presented an energetic approach to the study of inhomogeneous states (patterns) in systems with competing short-range attractive and long-range repulsive Coulomb interactions. Our approach becomes universal for systems with weak Coulomb interaction in the vicinity of the microphase separation transition, thus allowing us to treat a variety of physical situations which involve competing Coulomb interactions.

By the very definition of domain patterns, the width of the domain wall should be much smaller than the characteristic size of an individual domain. This requires that the Coulomb interaction be sufficiently weak in order for these patterns to be feasible. On the other hand, one can take advantage of this and study these patterns in the asymptotic limit of infinitely weak Coulomb interaction. This poses a challenge, however, since this interaction is a singular perturbation to the short-range interaction.

We have performed an asymptotic analysis of the free energy in the limit of vanishingly small strength of the Coulomb interaction ($\epsilon \to 0$). Our main finding is that in this limit the energetics of the patterns are described by the locations of the domain interfaces. In fact, an important hierarchy of length scales appears in the system [Eq. (16)]. Our second major observation is that the characteristic size of the domains in a stable domain pattern has to scale as $\epsilon^{-2/3}$. This is different from similar estimates based on the properties of *global* minimizers of the free energy [18,35,43,58,62]. What we showed in Sec. III B in general and Secs. IV C and IV D for particular patterns is that, unless this scaling is obeyed, the pattern cannot be a *local* minimizer and thus thermodynamically stable.

In our analysis, the starting point was the mean-field free energy functional from Eq. (1). We chose to perform our calculations using Eq. (5) for two reasons. First, this is a universal functional that is obtained in the vicinity of the microphase separation transition and therefore may be applied to a variety of systems. Second, using this functional we could obtain very explicit results, making our presentation more tractable. It is not difficult to see that all our calculations can be extended to the more general functional from Eq. (1). The only difference is that in the case of Eq. (1) the ''positive'' and ''negative'' domains may have asymmetric linear response coefficients $\kappa_{\pm}$ instead of a single κ in the case of Eq. (5). Nevertheless, in the case of Eq. (1) we can choose $\kappa = \kappa_+ f + \kappa_-(1-f)$, where f is the volume fraction of the ''positive'' domains (similar ideas were used in [60]). Indeed, since κ is responsible for screening, we can average the response of the order parameter on the scale of the domains, which is much smaller than the screening length (Sec. II B). The new definition of κ also takes into account that to leading order the (locally) averaged value of the volume fraction f is independent of space. The latter can be easily

seen from the analog of Eq. (36) obtained from Eq. (1), if one integrates this equation over a closed volume of size $\epsilon^{-2/3} \ll \ell \ll \epsilon^{-1}$, uses the Gauss theorem, and takes into account that ϕ is nearly constant in the domains and $|\nabla \psi| \sim \psi/R \sim \epsilon^{4/3}$ (see Sec. II C).

Let us point out that the interfacial representation of the free energy given by Eq. (29) which we obtained from the free energy functional in Eq. (5) in the asymptotic limit $\epsilon \to 0$ may in fact itself form a basis for studying the domain patterns in systems with long-range Coulomb interactions, provided that the driving force for the formation of these patterns is the competition of the Coulomb energy with the surface energy (see, for example, [12,15,35]). In this formulation our results can be applied to an even wider range of systems, which may not generally possess a free energy functional, like the one in Eq. (5). For example, our asymptotic results should apply to ferromagnetic nearest-neighbor Ising models frustrated by Coulomb interactions [30,32–34,36]. We argued that in these systems thermal fluctuations should only renormalize the effective coupling constant of the Coulomb interactions without qualitatively affecting the overall picture (Sec. II D). These predictions are difficult to compare with recent Monte Carlo simulations [33,34] because of the limitation of the latter on the system's size. Nevertheless, the result of [33] about the location of the microphase separation transition, which gives $\tau_c \sim \alpha^x$, with $x \simeq 0.25$–0.35, is not far from our prediction from Sec. II D of $\tau_c \sim \alpha^{0.40}$ for the three-dimensional Ising model. Note that we do not expect to find the avoided critical behavior discussed in the context of mean-spherical models [77].

An interesting question arising in systems with long-range competing interactions is the nature of the thermodynamic ground state below the microphase separation transition temperature. We emphasize that our stability analysis of stationary patterns only addresses small-scale thermal fluctuations, so we are really talking about *metastability* of these patterns. At the same time, rare large-scale thermal fluctuations may lead to nucleation or transitions between different metastable patterns (see Secs. V A and V C). In this sense, if there are enough metastable patterns, the global minimizer of the interfacial free energy, which is presumably a highly symmetric periodic pattern [18], has little to do with the thermodynamic ground state of the system.

In fact, we see that the stationary metastable patterns that form in one way or another are typically highly disordered (Sec. V C). Although the basic interaction between different domains is repulsion, the domains rarely arrange themselves in a close-packed fashion. The reason for that is that, even though the interaction between the domains is repulsive, the range of this interaction, which is determined by the screening length $L \sim \epsilon^{-1}$ is much greater than the characteristic interdomain distance $R \sim \epsilon^{-2/3}$. So a single domain interacts simultaneously with many other domains and not only with its nearest neighbors. Therefore, the optimization of the free energy becomes a collective problem, and a huge number of disordered metastable states appears. Then, the configurational entropy of these metastable disordered states may overwhelm their energy disadvantage [70,78].

Furthermore, a large-scale fluctuation whose size is comparable with the domain size $\sim R$ may propagate its action to a much larger distance $\sim L$ (see Fig. 9). It would seem natural to expect that, even if the system is in the lowest-energy state, a sufficiently strong fluctuation will frustrate a region much larger than the size of such a fluctuation, which may lead to increase of the degree of disorder with time. In this sense systems with long-range competing Coulomb interactions can be considered as *structural glasses* [30,37]. We emphasize that in these systems the disorder is self-induced. As we showed in Sec. V C, these systems can age on very long time scales and exhibit complex relaxation phenomena even in the case when the equations of motion for the patterns are very simple. Note that in a recent paper Schmalian and Wolynes came to similar conclusions on the basis of their replica analysis of Eq. (5) treated as an effective Hamiltonian [36]. Their calculations suggest that the number of metastable states grows exponentially with the system's volume, leading to an *ideal glass transition* below the microphase separation transition temperature. Also note that spin systems frustrated by Coulomb interactions have been proposed for studying glassy behavior in the supercooled liquids [79].

ACKNOWLEDGMENTS

The author would like to acknowledge many valuable discussions with E. Demler, W. Klein, and V. V. Osipov. The algebraic calculations of the paper benefited from the use of MATHEMATICA 4.0 software.

APPENDIX A: FREE ENERGY

Here we present the details of our manipulations of the interfacial free energy from Eq. (29) and the effective field ψ from Eq. (24). Let us first show the derivation of Eq. (28) from Eq. (27). In view of Eq. (24), we have

$$F_{\text{long range}} = \frac{1}{2} \int d^d x (\phi_{\text{sh}} - \overline{\phi}) \psi. \tag{A1}$$

According to Eq. (24) with $\phi_{\text{sh}} = \pm 1$, we have

$$\psi = -\epsilon^2 (1 + \overline{\phi}) \int d^d x' G_\epsilon (x - x') + 2\epsilon^2 \int_{\Omega_+} d^d x' G_\epsilon (x - x'), \tag{A2}$$

where the first integral is over the whole space. This integral is equal to $1/(\epsilon\kappa)^2$, according to Eq. (25). Substituting this back into Eq. (A1), after simple algebra we arrive at Eq. (28).

Let us now derive Eq. (29) from Eq. (28). Using Eq. (25) and applying Gauss's theorem, we calculate the long-range term:

$$2\epsilon^2\int_{\Omega_+}\int_{\Omega_+} d^dx\,d^dx' G_\epsilon(x-x') = \frac{2}{\kappa^2}\int_{\Omega_+}\int_{\Omega_+} d^dx d^dx' (\delta^{(d)}(x-x') + \nabla^2 G_\epsilon(x-x'))$$
$$= \frac{2}{\kappa^2}\int_{\Omega_+} d^dx + \frac{2}{\kappa^2}\int_{\Omega_+} d^dx' \oint dS\{\hat{n}\cdot\vec{\nabla} G_\epsilon(x-x')\}$$
$$\times\frac{2}{\kappa^2 d}\oint dS(\hat{n}\cdot\vec{x}) - \frac{2}{\kappa^2}\oint dS\int_{\Omega_+} d^dx'\vec{\nabla}'\cdot\{\hat{n}G_\epsilon(x-x')\}$$
$$= \frac{2}{\kappa^2 d}\oint dS(\hat{n}\cdot\vec{x}) - \frac{2}{\kappa^2}\oint dS\oint dS'(\hat{n}\cdot\hat{n}')G_\epsilon(x-x'). \tag{A3}$$

Let us now derive Eq. (39). Using Eq. (25), Eq. (A2), and Eq. (2) to express the δ function in terms of G, we get

$$\psi = -\frac{1+\overline{\phi}}{\kappa^2} + \frac{2}{\kappa^2}\int_{\Omega_+} d^dx'\nabla^2\{G_\epsilon(x-x') - G(x-x')\}$$
$$= -\frac{1+\overline{\phi}}{\kappa^2} + \frac{2}{\kappa^2}\oint dS'\{\hat{n}'\cdot\vec{\nabla}'(G_\epsilon - G)\}, \tag{A4}$$

where we applied Gauss's theorem.

Now let us calculate the first and second variations of the interfacial free energy. Let $\rho(x)$ be a normal displacement of the interface at point x on the interface, which is positive if the displacement is into the positive domain, and vice versa. Note that according to our definition $\rho>0$ corresponds to shrinking of Ω_+.

Up to second order in ρ, the change of the surface free energy $\Delta F_{\rm surf}$ is given by a well-known formula (see, for example, [80]):

$$\Delta F_{\rm surf} = -2\sigma_0\oint dS\,H\rho + \frac{\sigma_0}{2}\oint dS(|\vec{\nabla}_\perp\rho|^2 + 2K\rho^2), \tag{A5}$$

where H and K are mean and Gaussian curvatures at a given point of the interface, respectively, and $\vec{\nabla}_\perp$ denotes the gradient restricted to the interface. The mean curvature is positive if the positive domain is convex. The change of the long-range contributions to the free energy is given by the integral over a thin layer of thickness ρ over the interface. According to Eq. (28), we have

$$\Delta F_{\rm long\ range} = \frac{2(1+\overline{\phi})}{\kappa^2}\oint dS\int_0^{\rho(x)} dz(1-2Hz+Kz^2)$$
$$-4\epsilon^2\oint dS\int_0^{\rho(x)} dz(1-2Hz+Kz^2)$$
$$\times\int_{\Omega_+} d^dx' G_\epsilon(x-\hat{n}z-x')$$
$$+2\epsilon^2\oint dS\int_0^{\rho(x)} dz[1-2H(x)z+K(x)z^2]$$
$$\times\oint dS'\int_0^{\rho(x')} dz'[1-2H(x')z'+K(x')z'^2]$$
$$\times G_\epsilon(x-\hat{n}z-x'+\hat{n}'z'), \tag{A6}$$

where we used the fact that with our definition of the sign of the principal curvatures $d^dx = (1-k_1z)(1-k_2z)dzdS = (1-2Hz+Kz^2)dzdS$ at a point distance z away from the interface. Retaining only the terms up to second order in ρ and using Eq. (A2), we obtain

$$\Delta F_{\rm long\ range} = -2\oint dS\,\psi\rho + 2\oint dS\,H\psi\rho^2$$
$$+\oint dS\,(\hat{n}\cdot\vec{\nabla}\psi)\rho^2 + 2\epsilon^2\oint dS\oint dS'$$
$$\times G_\epsilon(x-x')\rho(x)\rho(x'), \tag{A7}$$

where we expanded ψ in a Taylor series in z. From this, and Eq. (A5), we get

$$\delta F = -2\oint dS(\sigma_0 H + \psi)\rho, \tag{A8}$$

so the critical points must satisfy Eq. (38). Similarly, using Eq. (38) in Eq. (A7), we obtain

$$\delta^2 F = \sigma_0\oint dS(|\vec{\nabla}_\perp\rho|^2 + 2K\rho^2) + \oint dS\{2(\hat{n}\cdot\vec{\nabla}\psi)$$
$$-4\sigma_0 H^2\}\rho^2 + 4\epsilon^2\oint dS\oint dS'$$
$$\times G_\epsilon(x-x')\rho(x)\rho(x'), \tag{A9}$$

which in view of Eq. (39) coincides with Eq. (41).

APPENDIX B: OPTIMAL PERIODS OF HEXAGONAL AND LAMELLAR PATTERNS

Here, we give the Wigner-Seitz calculation of the periods of hexagonal and lamellar patterns.

1. Hexagonal pattern

We start with a hexagonal pattern. Consider Eq. (23) on a disk of radius $\mathcal{R}=3^{1/4}\mathcal{L}_p/\sqrt{2\pi}$, with no-flux boundary conditions. Neglecting the term $\epsilon^2\kappa^2\psi$ and using Eq. (56), we write

$$\frac{d^2\psi}{dr^2}+\frac{1}{r}\frac{d\psi}{dr}+\epsilon^2\{\theta(\mathcal{R}_s-r) - \theta(r-\mathcal{R}_s)-2f+1\}=0, \tag{B1}$$

where r is the radial coordinate and $\theta(x)$ is the Heaviside step. The solution of this equation that satisfies Eq. (38) is given by

$$\psi=\begin{cases} \frac{1}{2}\epsilon^2\{(f-1)r^2+\mathcal{R}^2f(1-f)\}-\frac{1}{2}\sigma_0\mathcal{R}^{-1}f^{-1/2}, & 0\leqslant r\leqslant\mathcal{R}_s, \\ \frac{1}{2}\epsilon^2\{fr^2-f^2\mathcal{R}^2+f\mathcal{R}^2(\ln f\mathcal{R}^2-2\ln r)\}-\frac{1}{2}\sigma_0\mathcal{R}^{-1}f^{-1/2}, & \mathcal{R}_s\leqslant r\leqslant\mathcal{R}. \end{cases} \tag{B2}$$

where we took into account that $f=\mathcal{R}_s^2/\mathcal{R}^2$. According to Eq. (27) with $\phi_{\rm sh}=\pm 1$ and Eq. (A2), the long-range contribution to the free energy can be computed as

$$F_{\text{long range}}=(1-f)\int_{\Omega_+}\psi d^dx-f\int_{\Omega_-}\psi d^dx = 2\pi(1-f)\int_0^{\mathcal{R}_s}r\psi(r)dr-2\pi f\int_{\mathcal{R}_s}^{\mathcal{R}}r\psi(r)dr. \tag{B3}$$

Combining this with the surface energy $F_{\rm surf}=2\pi\sigma_0\mathcal{R}_s$ and using Eq. (B2), we get that the free energy per unit area is

$$\frac{F}{\pi\mathcal{R}^2}=\frac{2\sigma_0 f^{1/2}}{\mathcal{R}}+\frac{\epsilon^2\mathcal{R}^2f^2}{2}(f-1-\ln f), \tag{B4}$$

so, minimizing this expression with respect to $\mathcal{R}$ with fixed f, we obtain that the minimum is attained at $\mathcal{R}=\mathcal{R}^*$, where

$$\mathcal{R}^*=\epsilon^{-2/3}f^{-1/2}\left(\frac{2\sigma_0}{f-\ln f-1}\right)^{1/3}. \tag{B5}$$

Using the definition of $\mathcal{R}$ in terms of $\mathcal{L}_p$, this equation is rewritten as Eq. (58).

2. Lamellar pattern

Similarly, for the lamellar pattern centered at $x=0$ we get

$$\psi=\begin{cases} \epsilon^2(f-1)x^2+\frac{1}{4}\epsilon^2f^2(1-f)\mathcal{L}_p^2, & 0\leqslant x\leqslant\mathcal{L}_s/2, \\ \epsilon^2fx^2-\epsilon^2f\mathcal{L}_px+\frac{1}{4}\epsilon^2f^2(2-f)\mathcal{L}_p^2, & \mathcal{L}_s/2\leqslant x\leqslant\mathcal{L}_p/2, \end{cases} \tag{B6}$$

where we used the fact that $f=\mathcal{L}_s/\mathcal{L}_p$. Calculating the free energy per unit length, we get

$$\frac{F}{\mathcal{L}_p}=\frac{2\sigma_0}{\mathcal{L}_p}+\frac{1}{6}\epsilon^2\mathcal{L}_p^2f^2(1-f)^2. \tag{B7}$$

Minimizing this expression with respect to $\mathcal{L}_p$, we obtain Eq. (60).

APPENDIX C: STABILITY OF HEXAGONAL AND LAMELLAR PATTERNS

Here we present the details of our calculations of Eqs. (74) and (78).

1. Hexagonal pattern

We begin with the hexagonal pattern. We define

$$\mathsf{R}_{mm'}(\mathbf{k})=\frac{2\epsilon^2\mathcal{R}_s}{\pi}\sum_n\int_0^{2\pi}d\varphi\int_0^{2\pi}d\varphi' e^{im\varphi-im'\varphi'+i\mathbf{k}\cdot\mathbf{R}_n} \times G_\epsilon(\mathbf{R}_n+\mathbf{r}(\varphi')-\mathbf{r}(\varphi)), \tag{C1}$$

where $\mathbf{r}(\varphi)=(\mathcal{R}_s\cos\varphi,\mathcal{R}_s\sin\varphi)$ and the summation is over the lattice: $\mathbf{R}_n=n_1\mathbf{a}_1+n_2\mathbf{a}_2$, where $\mathbf{a}_1=\frac{1}{2}\mathcal{L}_p(\sqrt{3},1)$ and $\mathbf{a}_2=\frac{1}{2}\mathcal{L}_p(\sqrt{3},-1)$. Using the Fourier representation of $G_\epsilon(x-x')$, we obtain

$$\mathsf{R}_{mm'}(\mathbf{k}) = \frac{2\epsilon^2\mathcal{R}_s}{\pi}\sum_n \int_0^{2\pi} d\varphi \int_0^{2\pi} d\varphi' e^{im\varphi - im'\varphi'} \times \int \frac{d\mathbf{k}'}{(2\pi)^2} \frac{e^{i\mathbf{k}\cdot\mathbf{R}_n - i\mathbf{k}'\cdot[\mathbf{R}_n + \mathbf{r}(\varphi') - \mathbf{r}(\varphi)]}}{|\mathbf{k}'|^2 + \epsilon^2\kappa^2} \quad \text{(C2)}$$

$$= \frac{2\epsilon^2\mathcal{R}_s}{\pi v}\sum_n \int_0^{2\pi} d\varphi \int_0^{2\pi} d\varphi' e^{im\varphi - im'\varphi'} \times \frac{e^{i(\mathbf{k}+\mathbf{k}_n)\cdot(\mathbf{r}(\varphi) - \mathbf{r}(\varphi'))}}{|\mathbf{k}+\mathbf{k}_n|^2 + \epsilon^2\kappa^2}, \quad \text{(C3)}$$

where $v = \mathcal{L}_p^2\sqrt{3}/2$ is the area of the Wigner-Seitz cell (the sum is now over the reciprocal lattice), and we took into account that $\Sigma_n e^{i(\mathbf{k}-\mathbf{k}')\cdot\mathbf{R}_n} = (4\pi^2/v)\Sigma_n \delta(\mathbf{k}' - \mathbf{k} - \mathbf{k}_n)$.

We proceed:

$$\begin{aligned}\mathsf{R}_{mm'}(\mathbf{k}) &= \frac{2\epsilon^2\mathcal{R}_s}{\pi v}\sum_n \frac{1}{|\mathbf{k}+\mathbf{k}_n|^2 + \epsilon^2\kappa^2} \times \int_0^{2\pi} d\varphi e^{im\varphi + i(\mathbf{k}+\mathbf{k}_n)\cdot\mathbf{r}(\varphi)} \times \int_0^{2\pi} d\varphi' e^{-im'\varphi' - i(\mathbf{k}+\mathbf{k}_n)\cdot\mathbf{r}(\varphi')} \\ &= \frac{2\epsilon^2\mathcal{R}_s}{\pi v}\sum_n \frac{1}{|\mathbf{k}+\mathbf{k}_n|^2 + \epsilon^2\kappa^2} \times \int_0^{2\pi} d\varphi e^{im\varphi + i|\mathbf{k}+\mathbf{k}_n|\mathcal{R}_s\cos(\varphi - \vartheta_{\mathbf{k}+\mathbf{k}_n})} \times \int_0^{2\pi} d\varphi' e^{-im'\varphi' - i|\mathbf{k}+\mathbf{k}_n|\mathcal{R}_s\cos(\varphi' - \vartheta_{\mathbf{k}+\mathbf{k}_n})} \\ &= \frac{8\pi\epsilon^2\mathcal{R}_s}{v}\sum_n \frac{e^{i(m-m')\vartheta_{\mathbf{k}+\mathbf{k}_n}}}{|\mathbf{k}+\mathbf{k}_n|^2 + \epsilon^2\kappa^2} i^m J_m(|\mathbf{k} + \mathbf{k}_n|\mathcal{R}_s) i^{-m'} J_{m'}(|\mathbf{k}+\mathbf{k}_n|\mathcal{R}_s), \end{aligned} \quad \text{(C4)}$$

where we introduced the angle $\vartheta_{\mathbf{k}+\mathbf{k}_n}$ between the vector $\mathbf{k} + \mathbf{k}_n$ and the x axis and used the integral representation of the Bessel function. After a few algebraic manipulations, this equation can be converted to Eq. (75). Using the reciprocal lattice vectors $\mathbf{b}_1 = 2\pi\mathcal{L}_p^{-1}(1/\sqrt{3}, 1)$ and $\mathbf{b}_2 = 2\pi\mathcal{L}_p^{-1}(1/\sqrt{3}, -1)$, so $\mathbf{k}_n = n_1\mathbf{b}_1 + n_2\mathbf{b}_2$, this sum can be evaluated numerically by truncating the summation at sufficiently large $|n_1|$ and $|n_2|$.

An alternative representation for $\mathsf{R}_{mm'}(\mathbf{k})$, which allows us to explicitly calculate its diagonal elements, can be obtained by performing the summation in real space, rather than over the reciprocal lattice. We rewrite Eq. (C2) as

$$\begin{aligned}\mathsf{R}_{mm'}(\mathbf{k}) &= 4\epsilon^2\mathcal{R}_s\sum_n e^{i\mathbf{k}\cdot\mathbf{R}_n}\int_0^\infty \frac{qdq}{q^2+\epsilon^2\kappa^2} \times \int_0^{2\pi}\frac{d\vartheta}{2\pi} e^{-iq|\mathbf{R}_n|\cos(\vartheta - \vartheta_n)} \times \int_0^{2\pi}\frac{d\varphi}{2\pi} e^{im\varphi + iq\mathcal{R}_s\cos(\varphi - \vartheta)} \times \int_0^{2\pi}\frac{d\varphi'}{2\pi} e^{-im'\varphi' - iq\mathcal{R}_s\cos(\varphi' - \vartheta)} \\ &= 4\epsilon^2\mathcal{R}_s\sum_n e^{i\mathbf{k}\cdot\mathbf{R}_n}\int_0^\infty \frac{qdq}{q^2+\epsilon^2\kappa^2} \times \int_0^{2\pi}\frac{d\vartheta}{2\pi} e^{-iq|\mathbf{R}_n|\cos(\vartheta - \vartheta_n) + i(m-m')\vartheta} \times i^{m-m'} J_m(q\mathcal{R}_s) J_{m'}(q\mathcal{R}_s), \end{aligned} \quad \text{(C5)}$$

where ϑ_n is the angle between $\mathbf{R}_n$ and the x axis. Calculating the integral over ϑ, we obtain

$$\mathsf{R}_{mm'}(\mathbf{k}) = 4\epsilon^2\mathcal{R}_s\sum_n e^{i\mathbf{k}\cdot\mathbf{R}_n + i(m-m')\vartheta_n} \times \int_0^\infty \frac{qdq}{q^2+\epsilon^2\kappa^2} J_{m-m'}(q|\mathbf{R}_n|) \times J_m(q\mathcal{R}_s) J_{m'}(q\mathcal{R}_s). \quad \text{(C6)}$$

In calculating $\mathsf{R}_{mm'}(\mathbf{k})$, to leading order in ϵ one can neglect the term $\epsilon^2\kappa^2$ in the denominator of Eq. (75) or Eq. (C6). Setting ϵ to zero, we can calculate the diagonal elements $\mathsf{R}_{mm}(\mathbf{k})$ for $m \geqslant 2$. After some algebra

$$\mathsf{R}_{mm}(\mathbf{k}) = \frac{2\epsilon^2\mathcal{R}_s}{m}, \quad \text{(C7)}$$

where we took into account that the integrals in Eq. (C6) all vanish for $\mathbf{R}_n \neq 0$. Thus, the diagonal elements $\mathsf{R}_{mm}(\mathbf{k})$ are independent of $\mathbf{k}$ and coincide with those of a single spot.

Caution, however, is necessary when $|\mathbf{k}| \lesssim \epsilon$. In this case the $\mathbf{k}_n = 0$ contribution to the sum in Eq. (75) will be singular for $m, m' = 0, \pm 1$. Taking only the contribution of $\mathbf{k}_n = 0$, for $|\mathbf{k}| \ll 1$ we obtain

$$\mathsf{R}_{0,0}(\mathbf{k}) = \frac{16\pi\epsilon^2\mathcal{R}_s}{\mathcal{L}_p^2\sqrt{3}}\left(\frac{1}{|\mathbf{k}|^2 + \epsilon^2\kappa^2}\right), \quad \text{(C8)}$$

where we expanded the Bessel functions in a Taylor series and retained only the leading term. Now, to calculate $\mathsf{R}_{1,1}(\mathbf{k})$ for $\mathbf{k} = 0$, note that if one formally sets $\epsilon = 0$ in Eq. (75) with $m = m' = 1$, one should get the result of Eq. (C7). On the other hand, for $\mathbf{k} = 0$ the term with $\mathbf{k}_n = 0$ does not contrib-

ute, while for other $\mathbf{k}_n$ the term $\epsilon^2\kappa^2$ in Eq. (75) is a regular perturbation and can be neglected. So to calculate $\mathsf{R}_{1,1}(\mathbf{k})$ in the limit $|\mathbf{k}|\to 0$, one has to subtract the $\epsilon\to 0$ limit of the $\mathbf{k}_n=0$ term in Eq. (75) from Eq. (C7). As a result, we obtain

$$\mathsf{R}_{1,1}(0)=2\epsilon^2\mathcal{R}_s-\frac{4\pi\epsilon^2\mathcal{R}_s^3}{\mathcal{L}_p^2\sqrt{3}}, \tag{C9}$$

where we expanded the Bessel functions in a Taylor series and retained only the leading term.

Since $\mathsf{R}_{0,0}(\mathbf{k})\gg|\mathsf{R}_{mm'}(\mathbf{k})|$ for $m,m'\neq 0$ and small $|\mathbf{k}|$, the $m=0$ mode is the eigenfunction of the operator L in Eq. (42) for vanishing $|\mathbf{k}|$. The analysis of Eq. (74) with $m=m'=0$ and $\mathsf{R}_{0,0}(\mathbf{k})$ from Eq. (C8) shows that the hexagonal pattern is stable with respect to the long-wave modulation of the spots' radii, as long as $\mathcal{L}_p$ is large enough.

2. Lamellar pattern

Let us now turn to the lamellar pattern. Calculate the matrix elements of $4\epsilon^2G_\epsilon(x-x')$ between the right ("+") and left ("−") walls of the stripe in the zeroth period for a given modulation:

$$\begin{aligned}\langle+|4\epsilon^2G_\epsilon|+\rangle&=\langle-|4\epsilon^2G_\epsilon|-\rangle\\&=\frac{2\epsilon^2}{k}\sum_{n=-\infty}^{+\infty}e^{-k|\mathcal{L}_pn|+ik_\parallel n\mathcal{L}_p}\\&=\frac{2\epsilon^2e^{ik_\parallel\mathcal{L}_p}(e^{2k\mathcal{L}_p}-1)}{k(e^{(k+ik_\parallel)\mathcal{L}_p}-1)(e^{k\mathcal{L}_p}-e^{ik_\parallel\mathcal{L}_p})}\end{aligned} \tag{C10}$$

and

$$\begin{aligned}\langle+|4\epsilon^2G_\epsilon|-\rangle&=\langle-|4\epsilon^2G_\epsilon|+\rangle^*\\&=\frac{2\epsilon^2}{k}\sum_{n=-\infty}^{+\infty}e^{-k|\mathcal{L}_pn-\mathcal{L}_s|+ik_\parallel n\mathcal{L}_p}\\&=\frac{2\epsilon^2e^{ik_\parallel\mathcal{L}_p-k\mathcal{L}_s}}{k}\\&\quad\times\left(\frac{e^{2k\mathcal{L}_s}}{e^{k\mathcal{L}_p}-e^{ik_\parallel\mathcal{L}_p}}+\frac{e^{k\mathcal{L}_p}}{e^{(k+ik_\parallel)\mathcal{L}_p}-1}\right),\end{aligned} \tag{C11}$$

where we introduced $k=\sqrt{\epsilon^2\kappa^2+k_\perp^2}$, used the fact that the Fourier transform of the Green's function G_ϵ in the transverse direction is given by $\exp(-k|z-z'|)/2k$, and summed geometric series. After some algebra, the 2×2 matrix $\mathsf{R}(k_\parallel,k_\perp)$ formed by these matrix elements can be transformed into the following form:

$$\mathsf{R}(k_\parallel,k_\perp)=\frac{4\epsilon^2e^{k\mathcal{L}_p}}{k(1-2e^{k\mathcal{L}_p}\cos k_\parallel\mathcal{L}_p+e^{2k\mathcal{L}_p})}\begin{pmatrix}\sinh k\mathcal{L}_p & \sinh[k(\mathcal{L}_p-\mathcal{L}_s)]+e^{ik_\parallel\mathcal{L}_p}\sinh k\mathcal{L}_s\\ \sinh[k(\mathcal{L}_p-\mathcal{L}_s)]+e^{-ik_\parallel\mathcal{L}_p}\sinh k\mathcal{L}_s & \sinh k\mathcal{L}_p\end{pmatrix}. \tag{C12}$$

This matrix can be easily diagonalized; after a few manipulations we arrive at Eq. (79). Then, Eq. (80) is obtained by setting $\lambda_0=-\mathsf{R}_-(0,0)$ and taking only the leading order terms. Note that for $k_\parallel=0$ or $k_\parallel=\pi/\mathcal{L}_p$ the fluctuations corresponding to $\lambda_\pm$ are symmetric and antisymmetric deformations of stripes.

To obtain the energy of the long-wave distortions of the lamellar pattern, we expand Eq. (78) with R_- into a series in $k_\parallel$ and $k_\perp$ and retain the terms up to quadratic in $k_\parallel$ and fourth order in $k_\perp$. Then, to leading order in ϵ, we get

$$\begin{aligned}\lambda_-\simeq\frac{1}{2}f^2(1-f)^2\epsilon^2\mathcal{L}_p^3k_\parallel^2+\left(\sigma_0-\frac{1}{6}f^2(1-f)^2\epsilon^2\mathcal{L}_p^3\right)k_\perp^2\\+\frac{1}{360}[f^2(1-f)^2(1+2f-2f^2)\epsilon^2\mathcal{L}_p^5]k_\perp^4,\end{aligned} \tag{C13}$$

where we used $\mathcal{L}_s/\mathcal{L}_p=f$. One can see that at $\mathcal{L}_p=\mathcal{L}_p^*$ given by Eq. (60) the coefficient of $k_\perp^2$ changes sign from positive at $\mathcal{L}_p<\mathcal{L}_p^*$ to negative at $\mathcal{L}_p>\mathcal{L}_p^*$, signifying an instability. At the same time, the coefficient of $k_\perp^4$ is positive for all $0<f<1$.

Let us now discuss the stability of the lamellar patterns in one dimension, which can be studied by looking at Eq. (78) with $k_\perp=0$. Setting $k_\perp=0$ and expanding in ϵ, after some algebra we obtain that to leading order

$$\begin{aligned}\lambda_-=\frac{2\epsilon^2\mathcal{L}_p}{1-\cos k_\parallel\mathcal{L}_p}[1-f+f^2+f(1-f)\cos k_\parallel\mathcal{L}_p\\-\sqrt{1-2f(1-f)(1-\cos k_\parallel\mathcal{L}_p)}].\end{aligned} \tag{C14}$$

It is not difficult to verify that according to this equation $\lambda_-\geqslant 0$ for all values of $k_\parallel$, so the lamellar pattern is always stable regardless of the modulation vector $k_\parallel$ in one dimension. This conclusion is applicable when $\ln\epsilon^{-1}\ll\mathcal{L}_p\ll\epsilon^{-1}$, when the assumptions of the above equations are valid. Note that for $\mathcal{L}_p$ outside this range the one dimensional lamellar patterns (strata) may undergo a number of instabilities [2].

[1] M. Cross and P.C. Hohenberg, Rev. Mod. Phys. **65**, 851 (1993).

[2] B.S. Kerner and V.V. Osipov, *Autosolitons: A New Approach to Problems of Self-Organization and Turbulence* (Kluwer, Dordrecht, 1994).

[3] A.S. Mikhailov, *Foundations of Synergetics* (Springer-Verlag, Berlin, 1990).

[4] *Chemical Waves and Patterns*, edited by R. Kapral and K. Showalter (Kluwer, Dordrecht, 1995).

[5] *Nonlinear Dynamics and Pattern Formation in Semiconductors and Devices*, edited by F.J. Niedernostheide (Springer, Berlin, 1994).

[6] J.D. Murray, *Mathematical Biology* (Springer-Verlag, Berlin, 1989).

[7] M. Seul and D. Andelman, Science **267**, 476 (1995).

[8] T.H. O'Dell, *Ferromagnetodynamics: The Dynamics of Magnetic Bubbles, Domains, and Domain Walls* (Wiley, New York, 1981).

[9] *Ferroelectric Ceramics: Tutorial Reviews, Theory, Processing and Applications*, edited by N. Setter and E.L. Colla (Birkhauser, Basel, 1993).

[10] F.S. Bates and G.H. Fredrickson, Annu. Rev. Phys. Chem. **41**, 525 (1990).

[11] A.Y. Grosberg and A.R. Khokhlov, *Statistical Physics of Macromolecules* (AIP Press, New York, 1994).

[12] F.S. Bates and G.H. Fredrickson, Phys. Today **52**(2), 32 (1999).

[13] C.M. Care and N.H. March, Adv. Phys. **24**, 101 (1975).

[14] V.D. Kovalev and E.L. Nagaev, Sov. Phys. Usp. **29**, 297 (1986).

[15] E.L. Nagaev, Phys. Usp. **38**, 497 (1995).

[16] R.P. Huebener, *Magnetic Flux Structures in Superconductors* (Springer-Verlag, Berlin, 1979).

[17] L. Leibler, Macromolecules **13**, 1602 (1980).

[18] T. Ohta and K. Kawasaki, Macromolecules **19**, 2621 (1986).

[19] F. Liu and N. Goldenfeld, Phys. Rev. A **39**, 4805 (1989).

[20] I.Y. Erukhimovich and A.R. Khokhlov, Polym. Sci., Ser. A Ser. B **35**, 1522 (1993).

[21] V.Y. Borue and I.Y. Erukhimovich, Macromolecules **21**, 3240 (1988).

[22] I.A. Nyrkova, A.R. Khokhlov, and M. Doi, Macromolecules **27**, 4220 (1994).

[23] P.G. de Gennes, J. Phys. (France) Lett. **40**, 69 (1979).

[24] F.H. Stillinger, J. Chem. Phys. **78**, 4654 (1983).

[25] L.Q. Chen and A.G. Khachaturyan, Phys. Rev. Lett. **70**, 1477 (1993).

[26] S. Glotzer, E.A. Di Marzio, and M. Muthukumar, Phys. Rev. Lett. **74**, 2034 (1995).

[27] R.F. Mamin, JETP Lett. **60**, 52 (1994).

[28] C. Yeung and R.C. Desai, Phys. Rev. E **49**, 2096 (1994).

[29] M. Hildebrand, M. Kuperman, H. Wio, A.S. Mikhailov, and G. Ertl, Phys. Rev. Lett. **83**, 1475 (1999).

[30] V.J. Emery and S.A. Kivelson, Physica C **209**, 597 (1993).

[31] *Theory of Inhomogeneous Electron Gas*, edited by S. Lundqvist and N.H. March (Plenum Press, New York, 1983).

[32] U. Löw, V.J. Emery, K. Fabricius, and S.A. Kivelson, Phys. Rev. Lett. **72**, 1918 (1994).

[33] P. Viot and G. Tarjus, Europhys. Lett. **44**, 423 (1998).

[34] M. Grousson, G. Tarjus, and P. Viot, Phys. Rev. E **64**, 036109 (2001).

[35] J. Lorenzana, C. Castellani, and C. Di Castro, Phys. Rev. B **64**, 235127 (2001).

[36] J. Schmalian and P.G. Wolynes, Phys. Rev. Lett. **85**, 836 (2000).

[37] C.B. Muratov, Ph.D. thesis, Boston University, 1998.

[38] W.L. McMillian, Phys. Rev. B **12**, 1187 (1975).

[39] P. Hohenberg and W. Kohn, Phys. Rev. **136**, B864 (1964).

[40] J.R. Smith, Phys. Rev. **181**, 522 (1969).

[41] A.J. Bray, Adv. Phys. **43**, 357 (1994).

[42] L.D. Landau and E.M. Lifshits, *Course of Theoretical Physics* (Pergamon Press, London, 1980), Vol. 5.

[43] R. Choksi, J. Nonlinear Sci. **11**, 223 (2001).

[44] D.M. Petrich and R.E. Goldstein, Phys. Rev. Lett. **72**, 1120 (1994).

[45] R.E. Goldstein, D.J. Muraki, and D.M. Petrich, Phys. Rev. E **53**, 3933 (1996).

[46] L.D. Landau and E.M. Lifshits, *Course of Theoretical Physics* (Pergamon Press, London, 1984), Vol. 8.

[47] X.F. Ren and J.C. Wei, SIAM (Soc. Ind. Appl. Math.) J. Math. Anal. **31**, 909 (2000).

[48] C.B. Muratov, Phys. Rev. Lett. **78**, 3149 (1997).

[49] T. Ohta, A. Ito, and A. Tetsuka, Phys. Rev. A **42**, 3225 (1990).

[50] C.B. Muratov and V.V. Osipov, Phys. Rev. E **53**, 3101 (1996).

[51] T. Ohta, M. Mimura, and R. Kobayashi, Physica D **34**, 115 (1989).

[52] Y. Nishiura and H. Suzuki, SIAM (Soc. Ind. Appl. Math.) J. Appl. Math. **29**, 1087 (1998).

[53] A. Hagberg and E. Meron, Phys. Rev. Lett. **72**, 2494 (1994).

[54] A.B. Vasileva, V.F. Butuzov, and L.V. Kalachev, *The Boundary Function Method for Singular Perturbation Problems* (Society for Industrial and Applied Mathematics, Philadelphia, 1995).

[55] P.C. Fife, *Dynamics of Internal Layers and Diffusive Interfaces* (Society for Industrial and Applied Mathematics, Philadelphia, 1988).

[56] C.B. Muratov, Phys. Rev. E **54**, 3369 (1996).

[57] C.B. Muratov and V.V. Osipov, Phys. Rev. E **54**, 4860 (1996).

[58] I. Onishi, Y. Nishiura, M. Imai, and Y. Matsushita, Chaos **9**, 329 (1999).

[59] Y. Nishiura and I. Ohnishi, Physica D **84**, 31 (1995).

[60] C.B. Muratov, Phys. Rev. E **55**, 1463 (1997).

[61] J.M. Ziman, *Principles of the Theory of Solids* (Cambridge University Press, Cambridge, England, 1972).

[62] S. Müller, Calc. Var. Partial Differential Equations **1**, 169 (1993).

[63] L.M. Pismen, J. Chem. Phys. **101**, 3135 (1994).

[64] Lord Rayleigh, Philos. Mag. **14**, 184 (1882).

[65] X.F. Ren and J. C. Wei (unpublished).

[66] S. Qi and Z.-G. Wang, Macromolecules **30**, 4491 (1997).

[67] C. Yeung, A.-C. Shi, J. Noolandi, and R.C. Desai, Macromol. Theory Simul. **5**, 291 (1996).

[68] P.G. de Gennes and J. Prost, *The Physics of Liquid Crystals* (Oxford University Press, Oxford, 1993).

[69] Y. Oono and M. Bahiana, Phys. Rev. Lett. **61**, 1109 (1988).

[70] J.-P. Bouchaud, L.F. Cugliandolo, J. Kurchan, and M. Mézard, in *Spin Glasses and Random Fields*, edited by A. P. Young (World Scientific, Singapore, 1998).

[71] B. Meerson and P.V. Sasorov, Phys. Rev. E **53**, 3491 (1996).

[72] J. Rubinstein and P. Sternberg, IMA J. Appl. Math. **48**, 249 (1992).
[73] M. Bahiana and Y. Oono, Phys. Rev. A **41**, 6763 (1990).
[74] G. Coulon, B. Collin, and D. Chatenay, J. Phys. II **3**, 697 (1993).
[75] J.A. Cape and G.W. Lehman, J. Appl. Phys. **42**, 5732 (1971).
[76] W.M. Heckl and H. Möhwald, Ber. Bunsenges. Phys. Chem. **90**, 1159 (1986).
[77] L. Chayes, V.J. Emery, S.A. Kivelson, Z. Nussinov, and G. Tarjus, Physica A **225**, 129 (1996).
[78] D. Chowdhury, *Spin Glasses and Other Frustrated Systems* (Princeton University Press, Princeton, NJ, 1986).
[79] D. Kivelson, S.A. Kivelson, X. Zhao, Z. Nussinov, and G. Tarjus, Physica A **219**, 27 (1995).
[80] M.E. Taylor, *Partial Differential Equations III: Nonlinear Equations* (Springer-Verlag, Berlin, 1996).